

Phase Equilibria in Rocks of the Paleoproterozoic Banded Iron Formation (BIF) of the Lebedinskoe Deposit, Kursk Magnetic Anomaly, and the Petrogenesis of BIF with Alkali Amphiboles

K. A. Savko

Voronezh State University, Universitetskaya pl. 1, Voronezh, 394006 Russia

e-mail: ksavko@geol.vsu.ru

Received May 22, 2005

Abstract—BIF with alkali amphibole at the Lebedinskoe iron deposits, the largest in Russia, were metamorphosed at 550°C and 2–3 kbar and contain ferriwinchite, riebeckite, actinolite, grunerite, and aegirine–augite. All reaction textures observed in the rocks were produced during the prograde metamorphic stage and represent the following succession of mineral replacements: *Gru* → *Rbk*, *Act* → *Win* → *Rbk*. Data obtained on the textural relations and compositional variations of Ca, Ca–Na, and Na Al-free amphiboles point to the complete miscibility in the actinolite–ferriwinchite and ferriwinchite–riebeckite isomorphic series. Riebeckite is formed in BIF during the prograde metamorphic stage, with the participation of a fluid insignificantly enriched in Na⁺ and at increasing oxygen fugacity. The critical factors controlling the development of alkali amphiboles and Ca–Na pyroxenes in carbonate-bearing BIF is the oxygen activity and the presence of at least low concentrations of Na⁺ ions in the fluid. The minerals contain Fe³⁺, and all reactions producing them are oxidation reactions. The origin of riebeckite late in the course of the mineral-forming process is caused by the Ca²⁺Mg²⁺ → Na⁺Fe³⁺ heterovalent isomorphic replacement in calcic and calcic–sodic amphiboles and by the oxidation of grunerite in the presence of a fluid enriched in Na ions.

DOI: 10.1134/S086959110606004X

INTRODUCTION

Precambrian banded iron formations (BIF) are among the most mysterious rocks of the Earth. Although these rocks were extensively studied over a long time period, new and new geological phenomena are still discovered in them. It was previously believed that the rocks of BIF are characterized by a relatively simple mineralogical and chemical composition, which was controlled by the sedimentation conditions. Based on their chemistry and mineral assemblages, BIF are commonly subdivided into four major types (James, 1954): (i) quartz–magnetite (hematite) type, which is also sometimes referred to as the itabirite type and includes the *Qtz–Mag*, *Qtz–Hem*, and *Qtz–Hem–Mag* assemblages;¹ (ii) quartz–carbonate type, which contains much carbonates of the ferrodolomite–ankerite and siderite–pistomesite series; (iii) quartz–silicate type, which is dominated by quartz and ferro–ferric phyllosilicates: grinalite, menesotaite, chamosite, stilpnomelane, and, at higher metamorphic grades, also grunerite, hypersthene, and fayalite; and (iv) Mn-rich

BIF. Our data on the BIF of the Kursk Magnetic Anomaly (KMA) reveal a wealth of transitional varieties between the quartz–carbonate and quartz–silicate types, whose mineralogy is controlled by the proportions of K, Na, and Ca concentrations and the redox conditions during metamorphism.

This research was centered on the mineralogy and metamorphic processes of the rocks of the Paleoproterozoic BIF at Russia's largest Lebedinskoe iron deposit, KMA. Our earlier works at the Mikhailovskoe, Novoyaltinskoe, and Shemraevskoe iron deposits resulted in the distinguishing of a new mineralogical type of BIF, which is quantitatively dominated by potassic alumina-free micas: celadonite and tetraferri-biotite (Savko and Poskryakova, 2003a, 2003b, 2004). Our research whose results are summarized in this publication was centered on still another BIF type, which have never before been described in the literature, was found at the Lebedinskoe iron deposit, and contains ferriwinchite, a rare alumina-free sodic amphibole.

The aim of this paper is to interpret the systematic variations in the phase relations in BIF containing alkali amphiboles and to reproduce the physicochemical conditions under which these assemblages were formed.

¹ Mineral symbols: *Gru*—grunerite, *Rbk*—riebeckite, *Act*—actinolite, *Win*—winchite, *Qtz*—quartz, *Mag*—magnetite, *Hem*—hematite, *Aeg*—aegirine, *Aug*—augite, *Aeg–Aug*—aegirine–augite, *Dol*—dolomite, *Cal*—calcite, *Di*—diopside, *Grt*—garnet, *Bt*—biotite, *Ap*—apatite.

GEOLOGY

BIF in the Precambrian of KMA were found at three stratigraphic levels: Mesoarchean, Neoarchean, and Paleoproterozoic (Shchegolev, 1985). Paleoproterozoic BIF are spread the most widely at KMA and are ascribed to the Kursk Group. Their rocks extend for more than 550 km as two northwest-trending stripes: eastern Shchigrov–Oskol and western Mikhailovsk–Belgorod (Fig. 1). All of the currently developed iron deposits of the KMA basin are related to these Paleoproterozoic BIF.

The Lebedinskoe iron deposit is spatially restricted to the eastern Shchigrov–Oskol stripe in the southern closure of the Tim–Yastrebov riftogenic structure. The Precambrian rocks are overlain there by a Phanerozoic sedimentary cover up to 100–200 m thick. The Lebedinskoe deposit is hosted by potassic metarhyolites of the Neoarchean Lebedinskaya Formation (its magmatic zircon U–Pb age was estimated at 2590 ± 44 Ma; Shcherbak et al., 1992) and sedimentary–metamorphic rocks of the Paleoproterozoic Kursk Group, which is subdivided into the Stoilenskaya Formation and the overlying (without discernible unconformity) Korobkovskaya Formation (Fig. 1). The Stoilenskaya Formation composes the bottom of the Paleoproterozoic stratigraphic section of KMA, rests on a weathering crust of Neoarchean metarhyolites, and its rocks ubiquitously occur at the deposit. The formation is subdivided into upper schist and lower metasandstone subformations. The lower subformation (100–250 m thick) consists of quartzite-sandstones with a layer of metagritstone and metaconglomerate up to 3 m thick. The metasandstones include beds of high-Al schists of predominantly quartz–muscovite and muscovite–biotite composition, sometimes with garnet, up to 15 m thick. The upper schist subformation is made up of quartz–mica schists, sometimes with garnet and andalusite. Its thickness varies from 5 to 80 m.

The Korobkovskaya BIF formation has an overall thickness of 600 m and consists of two BIF subformations with two schist subformations in between (the latter are also referred to as intramineral schists). The formation conformably overlies the Stoilenskaya Formation (Fig. 1). Its lower boundary is conventionally drawn according to the first occurrence of grunerite quartzite layers. The lower BIF subformation ranges from 15 to 150 m in thickness and composes the peripheral parts of the deposit. It consists of magnetite quartzites, which often contain grunerite, ferriwinchite, and biotite. The lower schist subformation consists of dark gray quartz–biotite, biotite–garnet, and grunerite–biotite–garnet schists and has an average thickness of 60 m (at the Lebedinskoe deposit). The upper BIF subformation is 160–250 m thick and is composed of magnetite, grunerite–magnetite, biotite–magnetite, and riebeckite–ferriwinchite–magnetite quartzites, often with

calcite and dolomite and occasionally also with aegirine and aegirine-augite. The upper schist subformation is present only in the northwestern part of the deposit and is made up of quartz–mica and biotite–garnet schists, whose thicknesses significantly vary.

The magmatic rocks belong to the Stoilo–Nikolaevskii intrusive massif (4×9 km), which cuts across the BIF rocks in the northwestern portion of the deposit and has a zonal inner structure. Its peripheral zones consist of gabbro–diorites and diorites, which grade (through a zone of quartz diorites) into granodiorites of the central part of the massif. The U–Pb zircon age of the granodiorites is 2085 ± 5 Ma (Artemenko, 1998). The BIF are often intersected by diorite porphyry and granodiorite porphyry dikes up to 6 m thick (Fig. 2).

PETROGRAPHY AND PETROCHEMISTRY

The BIF of the Lebedinskoe deposit have a dark gray to greenish gray color, fine-grained texture, and banded structure, which is accentuated by alternating layers with magnetite (or, more rarely, hematite) and barren rocks (consisting of quartz, carbonates, amphiboles, and, occasionally, biotite) (Fig. 3). The magnetite layers are 0.3–0.7 cm thick and consist of cyclically alternating thin laminae of quartz and magnetite 0.5–1 mm thick. The quartz laminae are usually somewhat thicker than the magnetite laminae. The ore mineral of the ferriwinchite and grunerite BIF is magnetite. Hematite is rare and occurs only in rocks containing aegirine–augite.

Chemically, the BIF of the Lebedinskoe deposit (Table 1) correspond to the average compositions of BIF from other iron-ore basins (Gole and Klein, 1981) and differ from the quartzites of the western Mikhailovsk–Belgorod stripe in having higher alumina contents (0.98–2.35 wt % Al_2O_3) and lower $\text{Fe}^{3+}/(\text{Fe}^{3+} + \text{Fe}^{2+})$ ratios (0.53–0.58). The BIF of the Mikhailovskoe and Shemraevskoe deposits in the western stripe contain no more than 1 wt % Al_2O_3 and have $\text{Fe}^{3+}/(\text{Fe}^{3+} + \text{Fe}^{2+})$ ratios within the range of 0.70–0.87 (Savko and Poskryakova, 2003a, 2004). These features of the rocks were likely predetermined by the position of these BIF of the eastern and western stripes within the profile of sedimentation facies (Plaksenko, 1966). The Fe-rich sediments of the Lebedinskoe deposit were deposited closer to the shoreline than the sediments of the Mikhailovskoe deposit and contain more introduced terrigenous material. The chemistries of the BIF of these two large deposits also reflect the differences in their mineralogy: tetraferribiotite, celadonite, riebeckite, and aegirine in the BIF of the Mikhailovskoe deposit and ferriwinchite, aegirine-augite, and biotite in the BIF of the Lebedinskoe deposit.

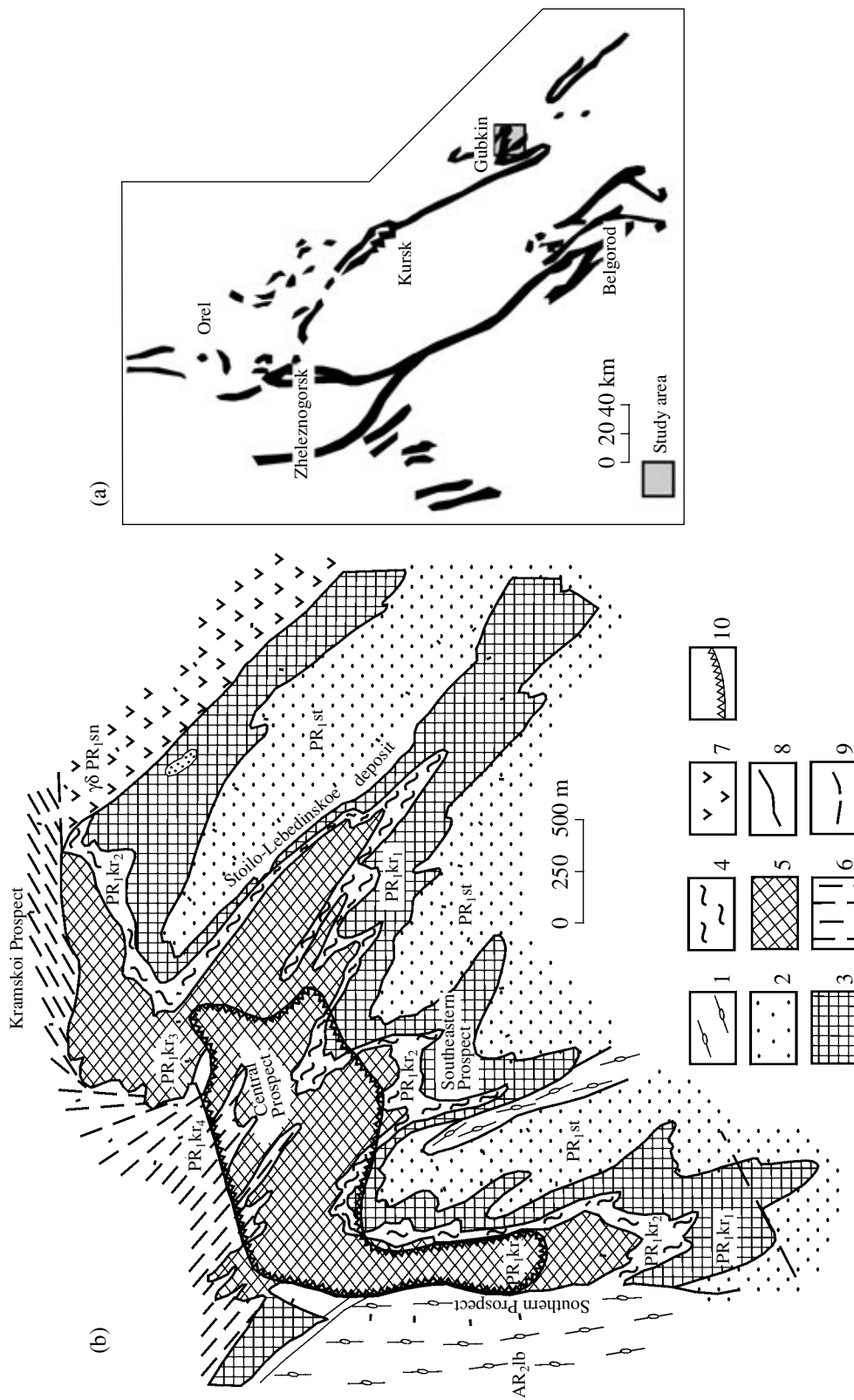


Fig. 1. Schematic geological map of (a) the Paleoproterozoic BIF of the Kursk Magnetic Anomaly (KMA) and (b) the Lebedinskoe iron deposit (modified after Iron Ores of KMA, 2001). Neoproterozoic: (1) quartz porphyries and rhyolites of the Lebedinskaya Formation (AR₂lb). Paleoproterozoic, Kursk Group: (2) aluminous schists, sandstones, and conglomerates in the bottom part of the Stoienskaya Formation (PR₁st); (3–6) Korobkovskaya Formation; (3) lower iron ore subformation (PR₁kr₁), (4) lower schist subformation (PR₁kr₂), (5) upper iron ore subformation (PR₁kr₃), (6) upper schist subformation (PR₁kr₄); (7) StoiLo-Nikolaevskii gabbro–diorte–granodiorite complex ($\gamma\delta$ PR₁sn); (8) geological boundaries; (9) faults; (10) contours of the opencast mine in projection onto the roof of the crystalline basement.



Fig. 2. Granodiorite porphyry dike in BIF, Lebedinskii opencast mine, northern wall, level -110 m.

METHODS

More than 100 samples of BIF and 20 intraminaler schists belonging to the Korobkovskaya Formation and the underlying schists of the Stoilenskaya Formation were collected in the walls of the opencast mine of the

Table 1. Average chemical composition (wt %) of BIF with alkali amphiboles from the Lebedinskoe deposit, KMA

Component	BIF with alkali amphiboles but without aegirine-augite ($n=6$)	BIF with alkali amphiboles and aegirine-augite ($n=5$)
SiO ₂	46.84	41.58
Al ₂ O ₃	2.35	0.98
TiO ₂	0.18	0.12
Fe ₂ O ₃	22.19	28.12
FeO	17.56	18.37
MgO	3.18	3.64
MnO	—	0.06
CaO	2.96	2.73
Na ₂ O	0.86	1.27
K ₂ O	0.71	0.29
P ₂ O ₅	0.10	0.10
S _{tot}	0.19	0.22
LOI	2.52	2.15
Total	99.64	99.93
Σ Fe	29.17	33.95
Fe ³⁺ /(Fe ³⁺ + Fe ²⁺)	0.53	0.58

Note: All analyses were conducted at the chemical laboratory of the Lebedinskii GOK JSC.



Fig. 3. BIF with alkaline amphiboles, sampling site L-5, Lebedinskii opencast mine, northern wall, level -110 m.

Dark gray layers consist of quartz and magnetite, pale gray layers are made up of ferriwinchite and aegirine-augite, very pale layers are composed of calcite and dolomite.

Lebedinskoe deposit during our fieldwork. The thin sections prepared of these samples were examined under a microscope. Spot analyses of minerals and BSE images were obtained on a CamScan electron microscope equipped with a Link EDS analytical set at the Institute of Experimental Mineralogy, Russian Academy of Sciences, at 20 kV accelerating voltage, a beam current of 1.2 mA, counting time of 70 s, and beam 1–3 μ m in diameter. The ZAF corrections were introduced during the calculation of oxide concentrations and the accuracy of the analyses was assayed by the installed software of the analytical system. The accuracy of analyses was systematically monitored by replicate analyses of natural and synthetic standards. The cation proportions (crystal-chemical formulae) were calculated by normalizing to four oxygen atoms for magnetite, twelve oxygen atoms for garnet, twenty-three oxygen atoms for amphiboles, six oxygen atoms for pyroxenes, and eleven oxygen atoms for biotite. The metamorphic temperatures were calculated by the TPF computer program (Fonarev et al., 1991). The numbers of analyses in the tables correspond to those of microprobe analyses shown in the figures.

MINERALOGY

Ca–Na Al-free amphiboles and their relations with other mineral phases in the BIF with alkali amphiboles were examined in detail on an electron microscope equipped with an energy-dispersive spectrometers (EDS). The rock samples were collected at the level of -110 m in the northern wall of the opencast mine (Fig. 3). The mineralogy of three of the most representative samples is described below.

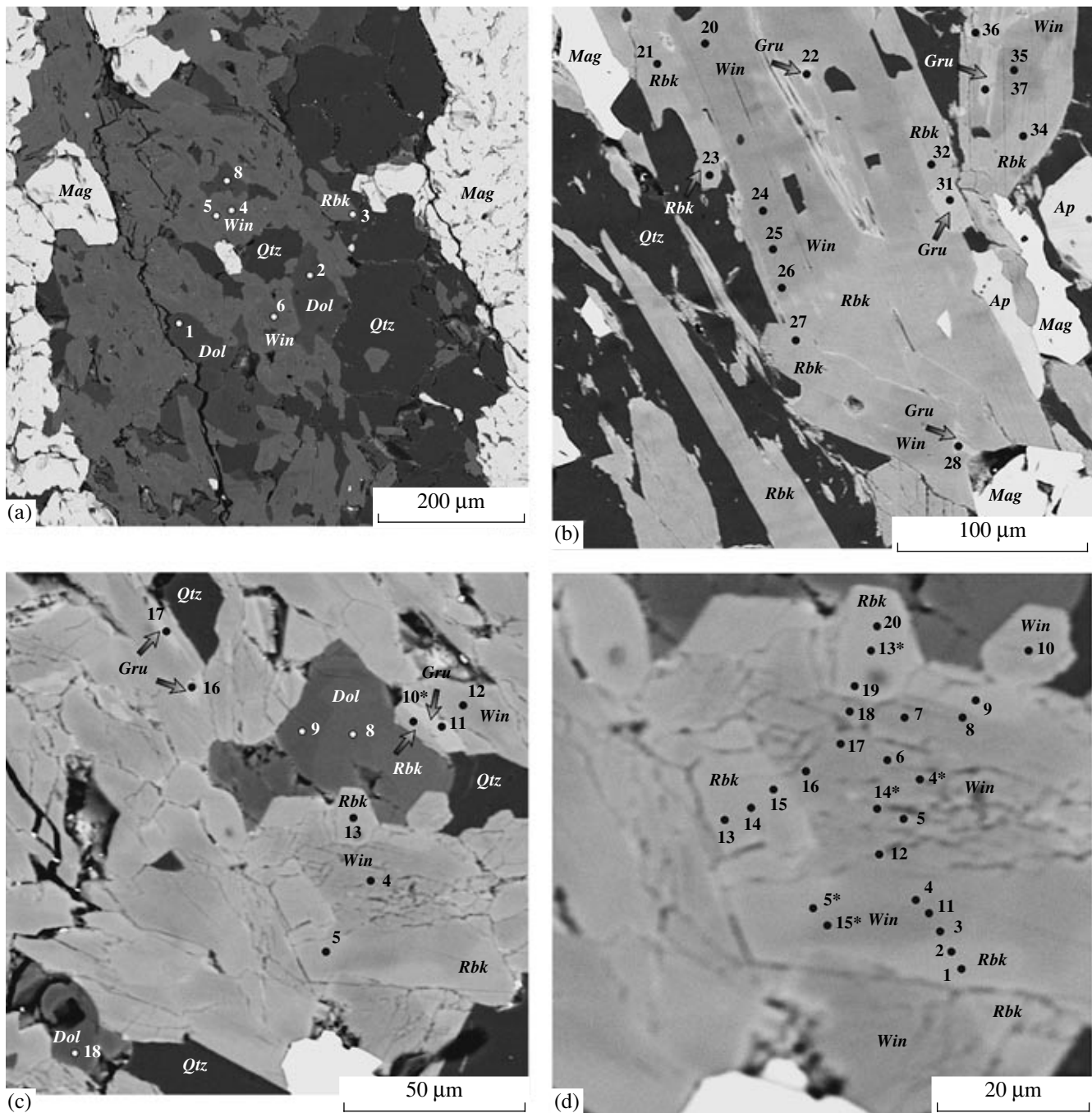


Fig. 4. Mineral assemblages and microprobe analytical spots in BIF with alkali amphiboles, sample L-5.

(a) Structure and texture of alkali amphibole layers; (b) relations between ferriwinchite (light), riebeckite (gray), and grunerite (pale gray): grunerite is preserved in zonal ferriwinchite–riebeckite crystals as fragments of paler color; (c) zonal ferriwinchite and dolomite crystals, grunerite relics in riebeckite; (d) zonal ferriwinchite crystal with an outermost riebeckite zone (analytical spots 1, 2, pale gray), intermediate zone (spots 3, 4, 11, and 15*, this zone is present fragmentarily and only in large crystals), and cores of the least sodic ferriwinchite (spots 5, 6, 17, and others, dark gray).

Sample L-5

Ferriwinchite occurs in this rock in the form of elongated prismatic and tabular crystals of pale blue color and with clear pleochroism in pale green shades. The crystals usually show a zonal distribution of their color:

their marginal portions (particularly the tops of the prisms) are of brighter color and pleochroic from pale to dark blue, which testifies to an increase in the Na concentration in the ferriwinchite and its transition to riebeckite. Most of the amphibole grains are relatively small, no longer than 50 μm, with crystals as large as

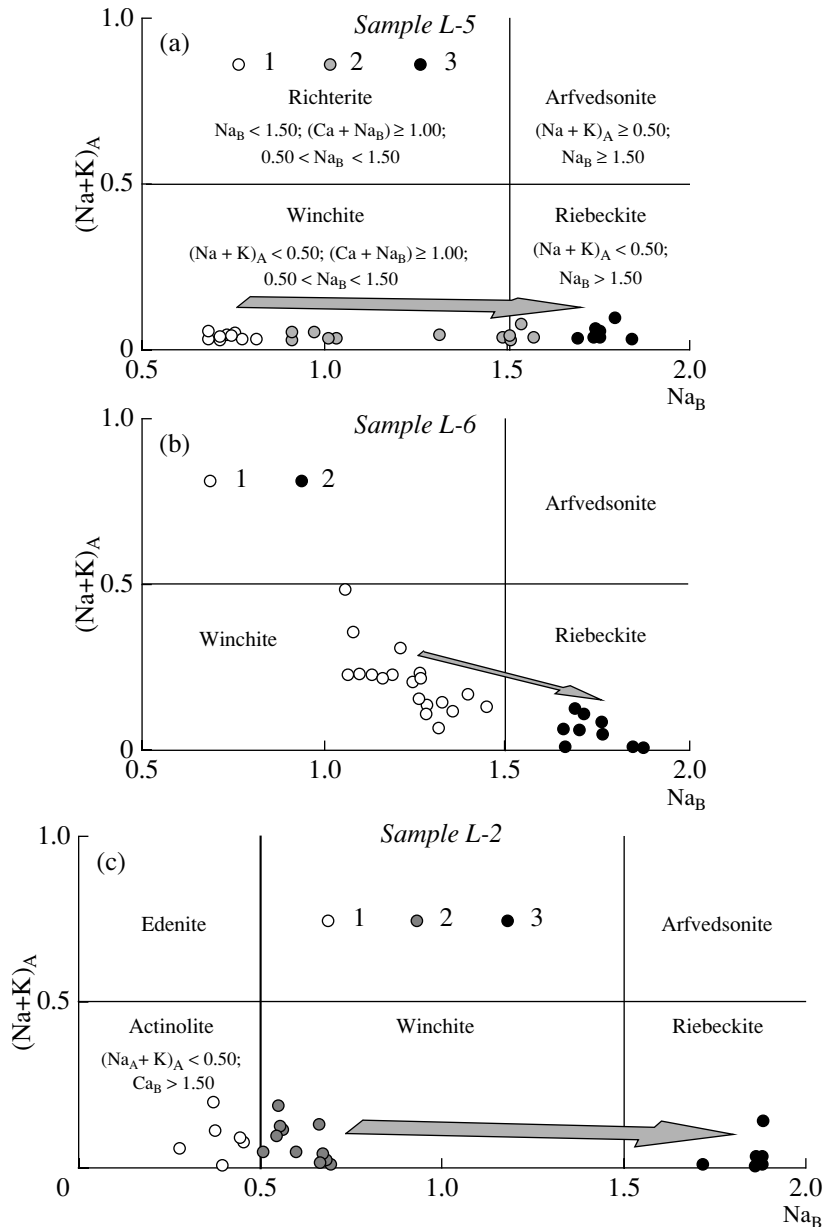


Fig. 5. $(\text{Na} + \text{K})_A$ vs. Na_B diagram for amphiboles from BIF with alkali amphiboles.

(a) Sample L-5: (1) crystal cores; (2) intermediate zones; (3) outer zones (see Fig. 4d). (b) Sample L-6: (1) crystal cores; (2) outer zones. (c) Sample L-2: (1) crystal cores; (2) outer zones; (3) riebeckite and riebeckite rims. Compositional fields are given after (Leake et al., 1997).

100–200 μm occurring only occasionally. The ferriwinchite composes thin, 0.5–1 mm thick, laminae between thicker quartz and magnetite layers and also occurs in magnetite or quartz layers in close association with dolomite (Fig. 4a).

Ferriwinchite crystals are zonal (both optically and compositionally; Figs. 4b, 4c). The BSE images of sample L-5 display three zones of these crystals: an outermost zone, intermediate zone, and core. The outermost zone is 10–15 μm thick, is paler, and consists of riebeckite (Figs. 4d, 5a, analytical spots 1, 2, 9, 14, and

15 and the corresponding analyses in Table 2). At one spot near the boundary with riebeckite (spot 13), the amphibole is ferriwinchite with 1.29 f.u. of Na (Fig. 4d). The inner zone is darker and was detected only in relatively large crystals, in which it occurs not ubiquitously (Figs. 4c, 4d), is 10–30 μm thick, and corresponds to ferriwinchite in composition (Fig. 4d, analytical spots 3, 4, 11, 5*, and 15*) with a fairly high concentration of Na (from 0.92 to 1.50 f.u.) and a low Ca content (0.46–1.08 f.u.). The concentration of Fe^{3+} decreases and those of Fe^{2+} and Mg increase within

both the inner and outer zones toward the core (Table 2). The systematic compositional variation of the amphiboles in sample L-5 are illustrated in $(\text{Na} + \text{K})_{\text{A}}-\text{Na}_{\text{B}}$ (Fig. 5a) and $(\text{Na} + \text{K} + \text{Fe}^{3+} + \text{Al}^{\text{VI}})-(\text{Ca}-\text{Mg}-\text{Fe}^{2+})$ (Fig. 6a) diagrams.

The cores of the crystals (darker in Figs. 4c and 4d) differ in composition from the inner parts, although they also consist of ferriwinchite. They are poorer in Na (0.7–0.8 f.u.; Fig. 7a) and Fe^{2+} (0.66–1.00 f.u.) but richer in Ca (1.18–1.30 f.u.) and Mg (3.0–3.3 f.u.) (Table 2, Fig. 6a).

Single small amphibole crystals have either riebeckite (spots 10* and 20) or ferriwinchite (spots 10 and 12*) compositions, which is typical of the internal zones of large crystals (Table 2).

The riebeckite zones of large ferriwinchite crystals contain small inclusions of grunerite relics with $X_{\text{Fe}} = 51\text{--}63$ at %. The inclusions are no larger than 15 μm , anhedral, and have diffuse uneven outlines (Figs. 6b, 6c).

The carbonate is dolomite, whose grains are also zonal: their X_{Fe} decreases from cores to margins (Table 3, Figs. 4a, 4c).

A widespread accessory mineral is F-apatite, which contains 1.4–4 wt % F (Fig. 4b).

Sample L-6

Large (up to 2–3 mm) prismatic crystals of ferriwinchite from sample L-6 (Fig. 7a) are also zonal: their outermost zones 20–50 μm thick consist of riebeckite, and the cores are the least sodic (Figs. 7b, 7c). In contrast to sample L-5, whose amphibole grains exhibit gradual transition from ferriwinchite to riebeckite, amphiboles in sample L-6 are characterized by a small compositional discontinuity in terms of Na concentration from ferriwinchite to riebeckite in the outer zones of large crystals (Figs. 5b, 6b). Moreover, ferriwinchite in this rock pervasively contains a K admixture, from 0.3 to 0.7 wt % K_2O (Table 4, Fig. 5b).

Aegirine-augite was found both in the matrix, in the form of small (30–40 μm) equant crystals (Fig. 7a), and in resorbed relicts in the cores of large ferriwinchite crystals (Figs. 7c, 7d). The latter are compositionally dominated by the acmite end member ($\text{Aeg}_{61\text{--}73}\text{Aug}_{27\text{--}39}$) (Table 5).

The only carbonate is calcite with low concentrations of MnO and FeO (Table 3).

Sample L-2

The BIF of sample L-2 contains amphibole laminae that are dominated by ferriwinchite and actinolite and bear strongly subordinate amounts of riebeckite (Figs. 8a, 8c). Unlike samples L-5 and L-6, whose BSE images exhibit a relatively smooth transition from ferriwinchite to riebeckite, sample L-2 is characterized by sharp contacts between riebeckite and ferriwinchite

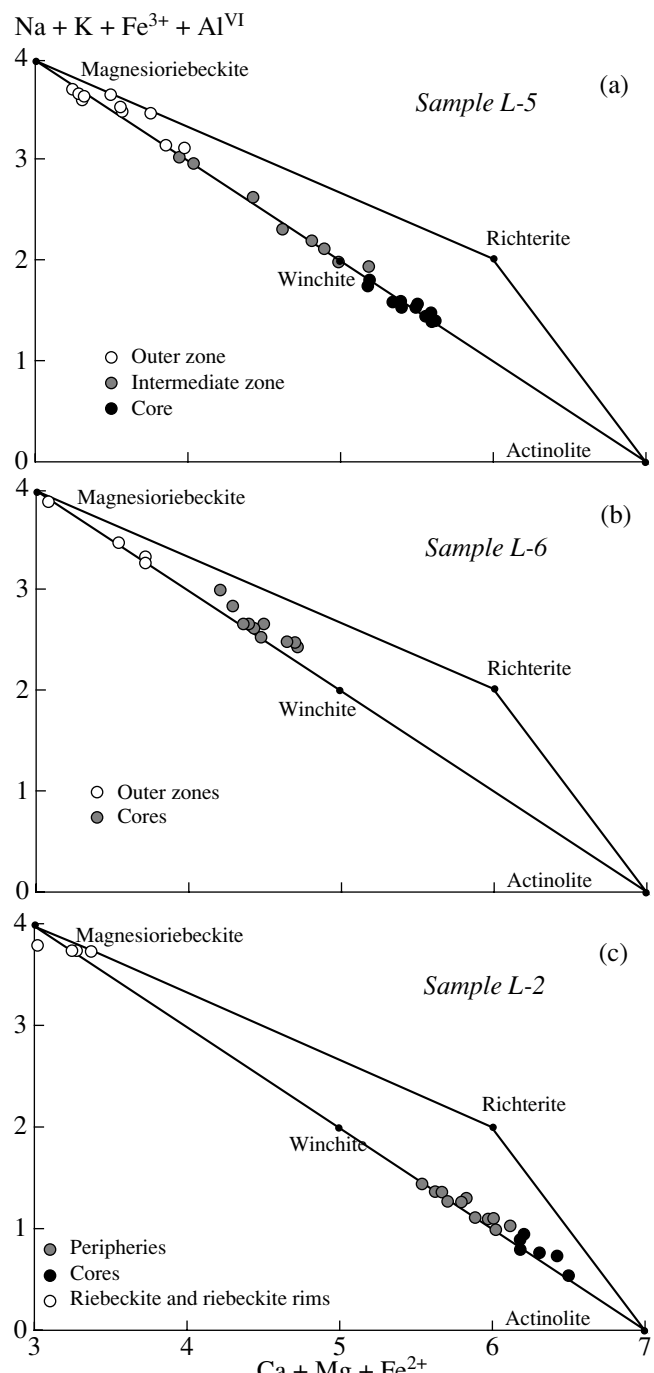


Fig. 6. $(\text{Na} + \text{K} + \text{Fe}^{3+} + \text{Al}^{\text{VI}})$ vs. $(\text{Ca} + \text{Mg} + \text{Fe}^{2+})$ diagram for amphiboles from BIF with alkali amphiboles.

(a) Sample L-5; (b) Sample L-6; (c) Sample L-2.

(Figs. 8d, 8e), and riebeckite forms small individual crystals (Fig. 8b). The cores of Ca-amphiboles in laminae between magnetite and quartz (or carbonate) layers consist of actinolite (Table 6, Figs. 5c, 6c). From cores to margins, their composition systematically varies and enriches in ferriwinchite, although this cannot be revealed microscopically. As can be seen in Figs. 5c

Table 2. Composition (wt %) of amphiboles from sample L-5

Component	Outer zone		Inner zone			Core margin	Inner core		
	Fig. 4d								
	Rbk-1	Rbk-2	Win-3	Win-11	Win-4	Win-12	Win-5	Win-4*	Win-6
SiO ₂ , at %	55.80	55.78	55.41	56.06	55.58	56.04	55.76	55.82	55.83
Al ₂ O ₃	0.74	—	0.58	—	—	—	—	0.51	—
FeO	24.15	24.75	18.32	16.95	17.05	16.62	15.36	15.94	15.69
MgO	9.57	9.45	13.57	14.52	14.25	14.66	15.28	14.76	15.13
CaO	1.55	1.63	6.12	6.92	7.07	7.58	8.31	8.30	8.39
Na ₂ O	5.68	6.36	3.71	3.34	3.31	2.79	2.80	2.44	2.46
K ₂ O	—	—	—	—	0.35	—	—	0.34	—
Total	97.49	97.97	97.71	97.79	97.61	97.69	97.51	98.11	97.50
Si, f.u.	7.96	8.01	7.86	7.94	7.94	7.94	7.94	7.91	7.94
Al ^{IV}	0.04	—	0.10	—	—	—	—	0.09	—
Fe ³⁺			0.04	0.06	0.06	0.06	0.06	—	0.06
ΣT	8.00	8.01	8.00	8.00	8.00	8.00	8.00	8.00	8.00
Al ^{VI}	0.08	—	—	—	—	—	—	—	—
Fe ³⁺	1.90	1.71	1.26	1.06	0.93	0.99	0.76	0.84	0.84
Fe ²⁺	0.97	1.26	0.88	0.89	1.05	0.91	1.00	1.05	0.96
Mg	2.03	2.02	2.87	3.06	3.03	3.09	3.24	3.12	3.20
ΣC	4.98	4.99	5.01	5.01	5.01	4.99	5.00	5.01	5.00
Ca	0.24	0.25	0.93	1.05	1.08	1.15	1.27	1.26	1.28
Na	1.57	1.75	1.02	0.92	0.92	0.77	0.73	0.67	0.68
ΣB	1.81	2.00	1.95	1.97	2.00	1.92	2.00	1.93	1.96
Na	—	0.02	—	—	—	—	0.04	—	—
K	—	—	—	—	0.06	—	—	0.06	—
ΣA	—	0.02	—	—	0.06	—	0.04	0.06	—
X _{Mg}	0.676	0.616	0.766	0.775	0.743	0.772	0.764	0.748	0.769
Component	Inner zone			Inner part of the crystal (core)					
	Fig. 4d								
	Win-13	Win-14	Win-15	Win-16	Win-17	Win-18	Win-7	Win-8	Win-14*
SiO ₂	54.94	55.50	55.30	55.66	55.85	56.56	55.96	55.15	54.96
Al ₂ O ₃	0.65	0.55	—	—	—	—	—	0.62	0.43
FeO	21.52	22.44	23.10	16.30	14.78	15.66	15.70	17.28	16.20
MgO	11.15	10.99	10.55	14.40	15.50	14.85	15.52	14.27	14.83
CaO	4.58	3.08	2.96	8.38	8.51	8.31	8.19	7.78	8.38
Na ₂ O	4.75	5.44	5.90	2.68	2.60	2.83	2.55	2.91	2.82
K ₂ O	—	—	—	0.28	0.26	—	0.38	—	0.30
Total	97.59	98.00	97.81	97.70	97.50	98.21	98.30	98.01	97.92
Si	7.91	7.91	7.96	7.98	7.95	8.01	7.89	7.83	7.84
Al ^{IV}	0.09	0.09	—	—	—	—	—	0.10	0.07
Fe ³⁺	—	—	0.04	0.02	0.05	—	0.11	0.07	0.09
ΣT	8.00	8.00	8.00	8.00	8.00	8.01	8.00	8.00	8.00
Al ^{VI}	0.02	—	—	—	—	—	—	—	—
Fe ³⁺	1.33	1.65	1.48	0.66	0.68	0.67	0.87	1.00	0.75
Fe ²⁺	1.26	1.02	1.26	1.27	1.03	1.18	0.87	0.98	1.09
Mg	2.39	2.33	2.26	3.07	3.29	3.13	3.26	3.02	3.15
ΣC	5.00	5.00	5.00	5.00	5.00	4.98	5.00	5.00	4.99
Ca	0.71	0.47	0.46	1.29	1.30	1.26	1.24	1.18	1.28
Na	1.29	1.50	1.54	0.71	0.70	0.74	0.70	0.80	0.72
ΣB	2.00	1.97	2.00	2.00	2.00	2.00	1.94	1.98	2.00
Na	0.04	—	0.11	0.03	0.02	0.04	—	—	0.06
K	—	—	—	—	—	—	—	—	—
ΣA	0.04	—	0.11	0.03	0.02	0.04	—	—	0.06
X _{Mg}	0.655	0.697	0.643	0.708	0.762	0.727	0.789	0.755	0.744

Table 2. (Contd.)

Component	Inner zone		Small grain			Outer zone	Core of a small grain	Matrix	Matrix	
	Fig. 4d							Fig. 4c		
	Win-5*	Win-15*	Rbk-13*	Rbk-19	Rbk-20	Rbk-9	Win-10	Win-12	Rbk-10	
SiO ₂	55.15	55.56	55.56	54.65	55.29	55.03	55.25	55.79	54.62	
Al ₂ O ₃	0.59	0.64	0.59	0.77	0.84	—	—	0.49	0.71	
FeO	23.07	22.45	25.01	25.09	23.71	24.51	20.57	18.29	24.87	
MgO	10.06	10.38	8.78	8.25	9.61	9.34	12.54	13.25	9.34	
CaO	3.21	3.38	1.14	1.06	1.60	1.67	6.26	6.47	1.37	
Na ₂ O	5.40	5.32	6.22	6.45	6.50	6.41	3.67	3.49	6.94	
K ₂ O	—	0.22	0.09	—	—	—	—	0.27	—	
Total	97.48	97.95	97.39	96.27	97.55	96.96	98.29	98.02	97.85	
Si	7.96	7.98	8.01	8.00	7.95	8.00	7.88	7.94	7.88	
Al ^{IV}	0.04	0.02	—	—	0.05	—	—	0.06	0.12	
Fe ³⁺	—	—	—	—	—	—	0.12	—	—	
ΣT	8.00	8.00	8.01	8.00	8.00	8.00	8.00	8.00	8.00	
Al ^{VI}	0.06	0.09	0.10	0.13	0.09	—	—	0.02	—	
Fe ³⁺	1.48	1.37	1.78	1.70	1.65	1.67	1.18	1.07	1.76	
Fe ²⁺	1.30	1.32	1.23	1.36	1.20	1.30	1.15	1.10	1.23	
Mg	2.16	2.22	1.88	1.80	2.06	2.02	2.67	2.81	2.01	
ΣC	5.00	5.00	4.99	4.99	5.00	4.99	5.00	5.00	5.00	
Ca	0.50	0.52	0.18	0.17	0.25	0.26	0.96	0.99	0.21	
Na	1.50	1.48	1.74	1.83	1.75	1.74	1.01	0.95	1.79	
ΣB	2.00	2.00	1.94	2.00	2.00	2.00	1.97	1.94	2.00	
Na	0.01	—	—	—	0.06	0.07	—	—	0.15	
K	—	0.04	—	—	—	—	—	0.05	—	
ΣA	0.01	0.04	—	—	0.06	0.07	—	0.05	0.15	
X _{Mg}	0.625	0.627	0.606	0.569	0.632	0.569	0.699	0.718	0.619	
Component	Fig. 4a		Fig. 4c			Fig. 4b				
	Win-6	Rbk-3	Gru-11	Gru-16	Gru-17	Gru-22	Gru-28	Gru-31	Gru-36	Gru-37
SiO ₂	55.32	55.06	53.46	53.80	54.20	53.90	53.55	53.78	53.37	53.95
Al ₂ O ₃	0.34	0.77	—	—	—	—	—	—	—	—
FeO	15.13	24.19	28.12	27.63	27.13	28.43	28.06	29.03	30.22	27.32
MnO	—	—	0.70	0.66	0.73	0.60	0.89	0.56	0.65	0.95
MgO	14.97	9.80	14.88	14.62	14.65	15.10	14.92	14.71	10.18	15.46
CaO	8.34	1.54	0.52	0.88	0.98	0.45	0.38	0.49	0.33	0.49
Na ₂ O	2.70	6.01	—	0.38	0.66	—	—	—	3.46	—
K ₂ O	0.34	—	—	—	—	—	—	—	—	—
Total	97.14	97.37	97.68	97.97	98.35	98.48	97.80	98.57	98.21	98.17
Si	7.93	7.89	8.00	8.00	8.00	8.00	8.00	7.99	7.90	8.00
Al ^{IV}	0.06	0.11	—	—	—	—	—	—	—	—
Fe ³⁺	0.01	—	—	—	—	—	—	0.01	0.10	—
ΣT	8.00	8.00	8.00	8.00	8.00	8.00	8.00	8.00	8.00	8.00
Al ^{VI}	—	0.02	—	—	—	—	—	—	—	—
Fe ³⁺	0.69	1.96	—	0.11	0.19	—	—	—	1.10	—
Fe ²⁺	1.11	0.94	3.51	3.32	3.16	3.51	3.50	3.59	2.54	3.38
Mn	—	—	0.09	0.08	0.09	0.08	0.11	0.07	0.08	0.12
Mg	3.20	2.09	3.32	3.24	3.22	3.34	3.32	3.26	2.24	3.42
ΣC	5.00	5.01	—	—	—	—	—	—	—	—
Ca	1.28	0.24	0.08	0.14	0.15	0.07	0.06	0.08	0.05	0.08
Na	0.72	1.67	—	0.11	0.19	—	—	—	0.99	—
ΣB	2.00	1.91	—	—	—	—	—	—	—	—
Na	0.03	—	—	0.11	0.19	—	—	—	0.99	—
K	0.06	—	—	—	—	—	—	—	—	—
ΣA	0.09	—	—	—	—	—	—	—	—	—
X _{Mg}	0.724	0.691	0.48	0.48	0.48	0.48	0.48	0.47	0.37	0.49

Table 2. (Contd.)

Component	Fig. 4b									
	Win-20	Rbk-21	Rbk-23	Win-24	Win-25	Win-26	Rbk-27	Rbk-32	Rbk-34	Win-35
SiO ₂	55.64	55.55	55.36	55.67	55.33	55.77	55.81	55.33	55.62	55.57
Al ₂ O ₃	0.57	0.51	0.56	0.19	0.43	0.42	0.82	0.39	0.43	0.33
FeO	16.88	23.51	23.39	15.56	16.12	16.82	24.80	24.18	24.29	16.79
MgO	14.27	10.28	10.26	14.87	14.74	13.80	9.38	10.14	9.67	14.23
CaO	7.86	2.30	2.83	8.35	8.36	7.99	1.21	2.54	2.26	8.08
Na ₂ O	3.14	5.62	5.33	2.90	2.97	2.78	5.89	5.56	5.77	2.75
K ₂ O	0.27	0.14	—	0.29	0.25	0.21	—	—	—	0.31
Total	98.63	97.91	97.73	97.83	98.20	97.79	97.91	98.14	98.04	98.06
Si	7.89	7.93	7.92	7.95	7.88	7.98	7.93	7.90	7.96	7.92
Al ^{IV}	0.10	0.07	0.08	0.03	0.07	0.02	0.07	0.07	0.04	0.06
Fe ³⁺	0.01	—	—	0.02	0.05	—	—	0.03	—	0.02
ΣT	8.00	8.00	8.00	8.00	8.00	8.00	8.00	8.00	8.00	8.00
Al ^{VI}	—	0.02	0.01	—	—	0.05	0.07	—	0.03	—
Fe ³⁺	0.82	1.78	1.71	0.64	0.70	0.71	2.01	1.80	1.71	0.79
Fe ²⁺	1.18	1.02	1.08	1.20	1.17	1.30	0.94	1.06	1.19	1.18
Mg	3.01	2.19	2.19	3.16	3.13	2.94	1.99	2.16	2.06	3.02
ΣC	5.01	5.01	4.99	5.00	5.00	5.00	5.01	5.02	4.99	4.99
Ca	1.19	0.35	0.43	1.28	1.28	1.22	0.18	0.39	0.35	1.23
Na	0.81	1.55	1.48	0.72	0.72	0.77	1.62	1.54	1.60	0.76
ΣB	2.00	1.90	1.91	2.00	2.00	1.99	1.80	1.93	1.95	1.99
Na	0.05	—	—	0.08	0.10	—	—	—	—	—
K	0.05	0.03	—	0.05	0.05	0.04	—	—	—	0.06
ΣA	0.10	0.03	—	0.13	0.15	0.04	—	—	—	0.06
X _{Mg}	0.719	0.681	0.669	0.726	0.728	0.694	0.679	0.671	0.633	0.718

Note: $X_{\text{Mg}} = \text{Mg}/(\text{Mg} + \text{Fe}^{2+})$.

and 6c, the amphibole compositions define a continuous isomorphic series from ferriwinchite to actinolite. The riebeckite has an unchanging composition and has low Ca concentrations. The carbonates are calcite and dolomite, which often occur in physical contact (Fig. 8f). Some large calcite crystals bear dolomite exsolution textures (Fig. 8f).

The BIF of sample L-2 also contains brownish biotite (Fig. 8f), which is low in alumina (10.8–11.3 wt % Al₂O₃) and has a high X_{Fe} (0.34–0.36) and approaches tetraferribiotite in composition.

METAMORPHIC P-T CONDITIONS

BIF usually contain no mineral sensors suitable for estimating the P - T metamorphic parameters, but the rock of sample L-2 contains abundant calcite and dolomite, which make it possible to assay the temperature,

using the compositions of these coexisting minerals, by the MgCO₃ concentration in the calcite (this concentration is a function of temperature on the calcite–dolomite solvus). The temperatures of metamorphic carbonate rocks can now be assayed by a number of versions of the calcite–dolomite thermometer. The version selected in this research accounts for the effect of additional components in the system (Table 7), although many researchers emphasized that one can be careful in applying this technique. The variations in the Mg concentrations in the calcite demonstrate fluctuations in the progress of the breakdown reactions of the solid solution. In order to obtain temperature close to the metamorphic peak, it was necessary to find calcite–dolomite pairs with the most magnesian calcite, whose degree of exsolution was insignificant.

Table 3. Composition (wt %) of carbonates in BIF from the Lebedinskoe deposit, KMA

Component	Sample L-5				Sample L-2							
	Fig. 4a		Fig. 4c		Fig. 8a	Fig. 8a	Fig. 8e	Fig. 8d	Fig. 8e	Fig. 8d	Fig. 8e	
	Dol-1	Dol-2	Dol-8	Dol-9	Dol-10	Dol-11	Cal-32	Dol-17	Cal-33	Dol-18	Cal-35	
FeO, wt %	14.50	18.74	17.86	14.86	13.92	10.97	2.65	12.70	2.30	11.57	3.32	
MnO	0.73	1.64	1.65	0.61	0.89	1.29	—	—	—	—	—	
MgO	29.69	25.55	26.35	29.61	29.90	31.22	2.05	30.45	1.77	31.35	1.80	
CaO	54.83	53.18	53.23	54.64	55.28	56.52	95.31	56.87	94.70	57.07	95.90	
Total	99.75	99.11	99.09	99.72	99.99	100.00	100.01	100.02	98.77	99.99	100.02	
Fe ²⁺ , f.u.	0.105	0.140	0.133	0.107	0.100	0.078	0.021	0.091	0.018	0.082	0.018	
Mn	0.005	0.012	0.012	0.004	0.006	0.009	—	—	—	—	—	
Mg	0.382	0.340	0.349	0.382	0.384	0.397	0.028	0.388	0.025	0.398	0.025	
Ca	0.508	0.508	0.506	0.506	0.510	0.516	0.951	0.521	0.957	0.520	0.957	
X _{Fe}	0.216	0.292	0.276	0.219	0.207	0.164	0.429	0.190	0.419	0.171	0.419	
Component	Sample L-2							Sample L-6				
	Fig. 8f							Fig. 7a				
	Dol-39	Dol-40	Cal-42	Dol-43	Dol-44	Cal-45	Dol-46	Cal-5	Cal-30	Cal-31		
FeO	13.78	14.49	1.43	16.23	12.09	1.26	14.48	1.48	1.53	1.04		
MnO	1.10	—	—	—	—	—	1.11	1.15	2.69	—		
MgO	29.48	30.32	1.37	28.46	30.38	1.08	18.54	—	—	—		
CaO	55.62	55.17	97.18	55.31	57.52	97.68	65.86	97.37	95.78	98.96		
Total	99.98	99.98	99.98	100.00	99.99	100.02	99.99	100.00	100.00	100.00		
Fe ²⁺	0.099	0.104	0.011	0.118	0.086	0.010	0.109	0.012	0.012	0.008		
Mn	0.008	—	—	—	—	—	0.008	0.009	0.012	—		
Mg	0.379	0.388	0.019	0.368	0.387	0.015	0.248	—	—	—		
Ca	0.514	0.508	0.970	0.514	0.527	0.975	0.634	0.979	0.966	0.992		
X _{Fe}	0.207	0.211	0.393	0.243	0.182	0.400	0.305	1.000	1.000	1.000		

Note: $X_{\text{Fe}} = \text{Fe}^{2+}/(\text{Mg} + \text{Fe}^{2+})$.

The temperatures estimated by the calcite–dolomite thermometer varied from 379 to 443°C (Table 7). These values of the metamorphic temperatures were tested by the garnet–biotite thermometer applied to the rocks of the lower schist subformation (intramineral schists), which are mostly quartz–biotite–garnet, quartz–biotite–andalusite, and quartz–biotite–grunerite–garnet schists. To quantify the temperature, we selected a quartz–biotite–grunerite–garnet schist (sample L-20)

with a very fine-grained matrix and large (3–4 mm across) garnet porphyroblasts (Fig. 9). The garnet cores contained numerous small inclusions of quartz, grunerite, and carbonaceous matter. The garnet was highly ferrous ($X_{\text{Fe}} = 0.930\text{--}0.961$), and its X_{Mg} increased from cores to margins (growth zoning, Table 8). It is interesting that this garnet contained no statistically significant amounts of Mn. The biotite was very fine-grained, occurred in intricately interlaced aggregates with

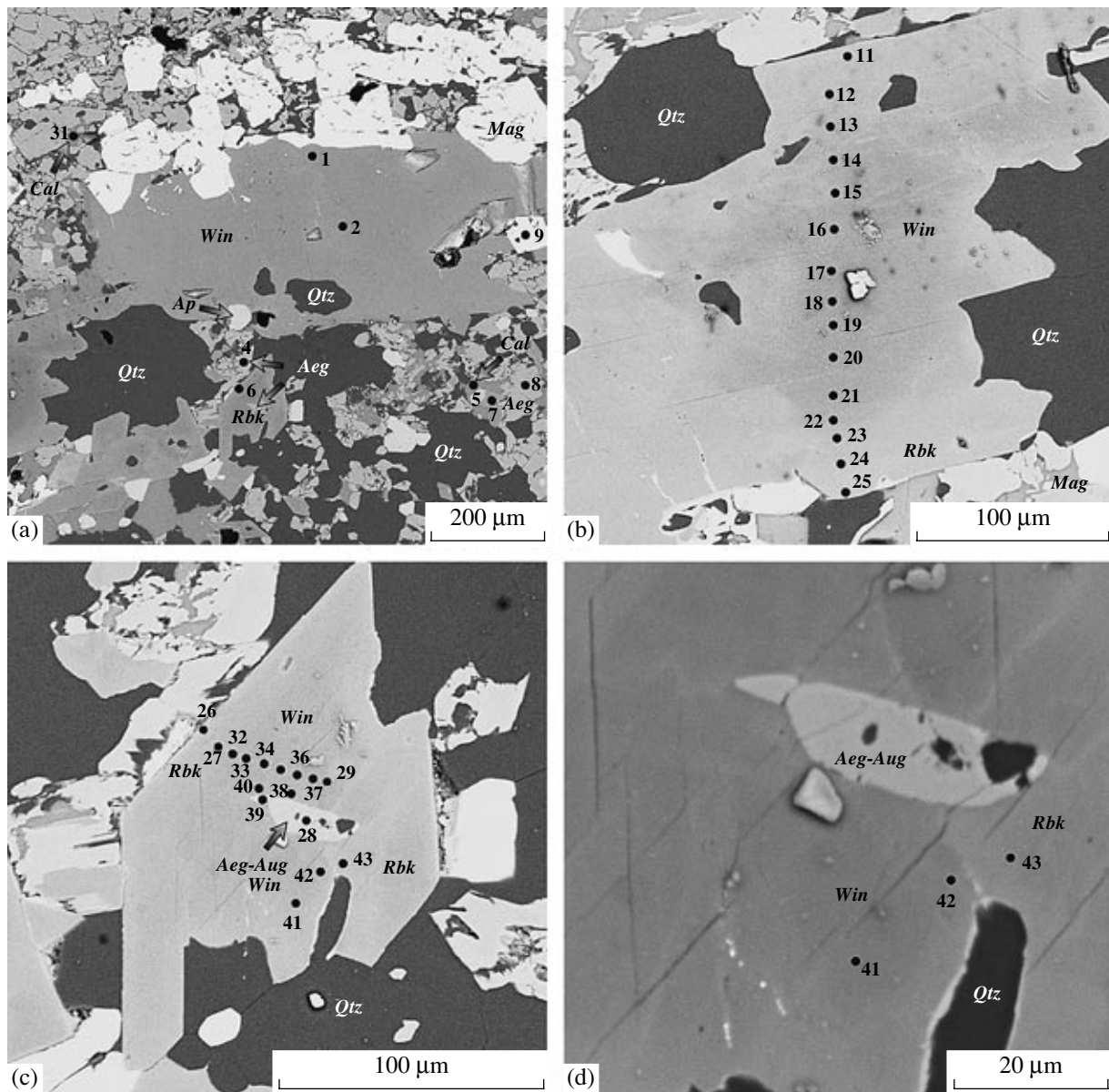


Fig. 7. Mineral assemblages and microprobe analytical spots in BIF with alkali amphiboles, sample L-6.

(a) Large prismatic riebeckite crystals that compose, together with aegirine-augite, interlayers between quartz and magnetite layers; (b) zonal ferriwinchite crystal with an outer riebeckite zone (spots 11, 12, and 23–25); (c) inclusion (relic) of aegirine-augite in a zonal ferriwinchite crystal; (d) relations between riebeckite and ferriwinchite zones in an amphibole crystal.

grunerite, and is highly aluminous and ferrous (Table 9). As can be seen from Table 10, the garnet–biotite thermometry of the intramineral schists yielded higher temperatures than those of the calcite–dolomite thermometry of the BIF: the cores of the garnet gave 485–500°C (early crystallization of the garnet), and the margins yielded 550°C (termination of garnet crystallization).

We failed to evaluate the pressures under which the intramineral schists were formed because they bear no mineral assemblages suitable for mineralogical barometry, but the fact that the mineral assemblages contained

andalusite at temperatures of 500–550°C indicates that the pressures were no higher than 3.5 kbar.

DISCUSSION

The results of our research were obtained in order to settle the following two problems: (i) whether there is a miscibility gap in the series of Ca-, Ca-Na, and Na-amphiboles in BIF and (ii) what were the metamorphic parameters under which the “subalkaline” BIF were produced.

Table 4. Composition (wt %) of amphiboles from sample L-6

Component	Fig. 7a				Fig. 7b					
	Rbk-1	Rbk-2	Rbk-6	Rbk-7	Rbk-11	Rbk-12	Win-13	Win-14	Win-15	
SiO ₂ , wt %	56.93	56.36	53.04	56.19	55.48	56.20	56.53	55.68	56.30	
Al ₂ O ₃	—	—	—	—	0.95	—	—	—	—	
FeO	21.68	22.57	36.80	21.98	21.84	20.69	16.80	16.70	16.37	
MgO	11.85	11.78	2.80	11.23	10.85	11.99	14.36	13.97	14.41	
CaO	0.70	0.82	0.41	1.14	1.27	1.92	4.82	5.14	5.29	
Na ₂ O	6.75	6.55	6.27	6.58	6.38	6.36	5.03	5.17	4.81	
K ₂ O	—	—	—	—	0.30	0.34	0.49	0.45	0.46	
Cl	—	—	—	—	—	—	—	—	—	
F	—	—	—	—	—	—	—	—	—	
Total	97.91	98.08	99.32	97.12	98.50	97.50	98.03	97.11	97.64	
Si, f.u.	7.99	7.90	7.84	8.00	7.93	8.00	7.99	8.00	8.00	
Al ^{IV}	—	—	—	—	0.07	—	—	—	—	
Fe ³⁺	0.01	0.10	0.16	—	—	—	0.01	—	—	
ΣT	8.00	8.00	8.00	8.00	8.00	8.00	8.00	8.00	8.00	
Al ^{VI}	—	—	—	—	0.09	—	—	—	—	
Fe ³⁺	1.97	2.08	2.23	1.83	1.78	1.60	1.08	0.89	0.97	
Fe ²⁺	0.55	0.46	2.15	0.78	0.83	0.86	0.89	1.12	0.97	
Mg	2.48	2.46	0.62	2.38	2.31	2.54	3.02	2.99	3.05	
ΣC	5.00	5.00	5.00	4.99	5.01	5.00	4.99	5.00	4.99	
Ca	0.11	0.12	0.06	0.17	0.19	0.29	0.73	0.79	0.81	
Na	1.83	1.78	1.80	1.82	1.77	1.71	1.27	1.21	1.19	
ΣB	1.94	1.90	1.86	1.99	1.96	2.00	2.00	2.00	2.00	
Na	—	—	—	—	—	0.04	0.11	0.23	0.13	
K	—	—	—	—	0.05	0.06	0.09	0.08	0.08	
ΣA	—	—	—	—	0.05	0.10	0.20	0.31	0.21	
Cl	—	—	—	—	—	—	—	—	—	
F	—	—	—	—	—	—	—	—	—	
X _{Mg}	0.817	0.841	0.223	0.752	0.736	0.748	0.772	0.728	0.758	
Component	Fig. 7b									
	Win-16	Win-17	Win-18	Win-19	Win-20	Win-21	Rbk-22	Rbk-23	Rbk-24	Rbk-25
SiO ₂	56.65	57.20	56.70	56.69	57.82	56.95	57.07	57.35	56.85	56.65
Al ₂ O ₃	—	—	—	—	—	—	—	—	—	—
FeO	13.74	12.97	12.69	12.26	12.55	13.05	19.91	21.35	24.16	24.27
MgO	16.09	16.73	16.65	16.92	17.33	16.60	13.01	12.97	10.46	10.40
CaO	6.17	5.77	6.06	6.28	6.18	5.57	1.68	1.41	0.54	0.56
Na ₂ O	4.38	4.65	4.77	5.16	4.50	4.58	6.54	6.12	6.80	6.82
K ₂ O	0.53	0.62	0.70	0.72	0.62	0.66	0.29	—	—	—
Cl	—	—	—	0.35	—	—	—	—	—	—
F	—	—	—	—	—	—	—	—	—	—
Total	97.56	97.94	97.57	98.03	99.00	97.41	98.50	99.20	98.81	98.70
Si	8.00	8.00	8.00	8.00	7.99	8.00	7.97	7.89	7.98	7.97
Al ^{IV}	—	—	—	—	—	—	—	—	—	—
Fe ³⁺	—	—	—	—	0.01	—	0.03	0.11	0.02	0.03
ΣT	8.00	8.00	8.00	8.00	8.00	8.00	8.00	8.00	8.00	8.00
Al ^{VI}	—	—	—	—	—	—	—	—	—	—
Fe ³⁺	0.85	0.90	0.73	0.56	0.87	0.97	1.70	2.06	2.01	2.00
Fe ²⁺	0.77	0.61	0.77	0.88	0.56	0.56	0.59	0.28	0.81	0.82
Mg	3.38	3.49	3.50	3.56	3.57	3.47	2.71	2.66	2.19	2.18
ΣC	5.00	5.00	5.00	5.00	5.00	5.00	5.00	5.00	5.01	5.00
Ca	0.93	0.86	0.92	0.95	0.91	0.84	0.25	0.21	0.08	0.08
Na	1.07	1.14	1.08	1.05	1.09	1.16	1.75	1.63	1.85	1.86
ΣB	2.00	2.00	2.00	2.00	2.00	2.00	2.00	1.84	1.93	1.94
Na	0.13	0.12	0.22	0.36	0.11	0.09	0.02	—	—	—
K	0.10	0.11	0.13	0.13	0.11	0.12	0.05	—	—	—
ΣA	0.23	0.23	0.35	0.49	0.22	0.21	0.07	—	—	—
Cl	—	—	—	0.08	—	—	—	—	—	—
F	—	—	—	—	—	—	—	—	—	—
X _{Mg}	0.814	0.850	0.821	0.801	0.864	0.860	0.821	0.905	0.731	0.727

Table 4. (Contd.)

Component	Fig. 7c										Fig. 7c	Fig. 7d		
	Rbk-26	Rbk-27	Win-32	Win-33	Win-34	Win-35	Win-36	Win-37	Win-29	Win-38	Win-40	Win-41	Win-42	Win-43
SiO ₂	56.69	56.42	56.96	57.10	57.08	56.78	56.16	57.11	56.62	55.91	56.69	56.30	56.66	56.81
Al ₂ O ₃	—	—	—	—	—	—	0.21	0.14	—	—	—	—	—	0.40
FeO	23.05	20.63	19.09	16.46	15.76	16.74	16.38	16.58	15.18	19.11	17.56	16.28	17.40	21.31
MgO	11.25	12.08	13.18	14.84	15.11	14.41	14.11	14.59	15.23	13.18	13.93	14.49	14.01	11.63
CaO	0.66	1.58	2.10	4.47	4.61	4.33	4.87	4.49	4.91	3.67	3.95	5.01	4.30	2.26
Na ₂ O	6.75	6.68	6.49	5.07	4.70	4.69	4.77	4.86	4.97	5.60	5.36	4.88	5.03	6.21
K ₂ O	—	—	0.16	0.51	0.67	0.50	0.52	0.41	0.60	0.39	0.43	0.59	0.44	0.17
Cl	—	—	—	—	—	—	0.18	0.08	—	—	—	—	—	—
F	—	—	—	—	—	—	—	0.60	—	0.55	—	—	—	—
Total	98.40	97.39	97.98	98.45	97.93	97.45	97.02	98.18	97.51	97.86	97.92	97.55	97.84	98.79
Si	7.95	8.00	8.00	7.99	8.00	8.00	8.01	8.00	8.00	7.94	8.00	8.00	8.00	7.99
Al ^{IV}	—	—	—	—	—	—	—	—	—	—	—	—	—	0.01
Fe ³⁺	0.05	—	—	0.01	—	—	—	—	—	0.06	—	—	—	—
ΣT	8.00	8.00	8.00	8.00	8.00	8.00	8.01	8.00	8.00	8.00	8.00	8.00	8.00	8.00
Al ^{VI}	—	—	—	—	—	—	0.04	0.02	—	—	—	—	—	0.06
Fe ³⁺	2.02	1.68	1.57	1.21	1.22	1.31	1.03	1.25	1.04	1.32	1.26	1.02	1.24	1.54
Fe ²⁺	0.63	0.77	0.67	0.70	0.63	0.66	0.92	0.69	0.75	0.88	0.81	0.91	0.81	0.96
Mg	2.35	2.55	2.76	3.09	3.15	3.03	3.00	3.04	3.21	2.79	2.93	3.07	2.95	2.44
ΣC	5.00	5.00	5.00	5.00	5.00	5.00	4.99	5.00	5.00	4.99	5.00	5.00	5.00	5.00
Ca	0.10	0.24	0.32	0.67	0.69	0.65	0.74	0.67	0.74	0.56	0.60	0.76	0.65	0.34
Na	1.83	1.76	1.68	1.33	1.28	1.28	1.26	1.32	1.26	1.44	1.40	1.24	1.35	1.66
ΣB	1.93	2.00	2.00	2.00	1.97	1.93	2.00	1.99	2.00	2.00	2.00	2.00	2.00	2.00
Na	—	0.08	0.09	0.04	—	—	0.06	—	0.10	0.10	0.07	0.10	0.03	0.03
K	—	—	0.03	0.09	0.12	0.09	0.09	0.07	0.11	0.07	0.08	0.11	0.08	0.03
ΣA	—	0.08	0.12	0.13	0.12	0.09	0.15	0.07	0.21	0.17	0.15	0.21	0.11	0.06
Cl	—	—	—	—	—	—	0.04	0.02	—	—	—	—	—	—
F	—	—	—	—	—	—	—	0.27	—	0.25	—	—	—	—
X _{Mg}	0.788	0.769	0.804	0.816	0.834	0.822	0.766	0.815	0.810	0.759	0.783	0.771	0.784	0.717

Miscibility in the Actinolite–Ferriwinchite and Ferriwinchite–Riebeckite Isomorphic Series

The textural relations, compositions, and zoning of the amphiboles suggest that the actinolite–ferriwinchite and ferriwinchite–riebeckite series are characterized by complete miscibility. Miscibility gaps in the series of

Ca–Na and Na amphiboles were documented for glaucophane and actinolite (Klein, 1969; Robinson et al., 1982; Reynard and Ballevre, 1988), glaucophane and grunerite (Smelik and Veblen, 1992), glaucophane and hornblende (Klein, 1969) glaucophane and barroisite (Robinson et al., 1982), hastingsite and ferricataphorite

(Shearer et al., 1981), and for richterite and magnesioriebeckite (Ghose et al., 1974). Our Ca–Na amphiboles display heterovalent isomorphism $\text{Ca}^{2+}\text{Mg}^{2+} \rightarrow \text{Na}^+\text{Fe}^{3+}$. As can be seen in Figs. 5a and 6a, the transition from ferriwinchite to riebeckite has no compositional gaps in the isomorphic series. The situation with the transition from actinolite to ferriwinchite is analogous (Figs. 5c, 6c). This definitely indicates that the amphibole series in question is characterized by complete miscibility. The reasons for the “leaps” and “discontinuities” in the Na concentration detected in some samples with the transition from ferriwinchite to riebeckite can be of kinetic nature.

Petrogenesis of Alkali-Amphibole BIF at KMA

Alkali-rich rocks of Precambrian BIF are common in Precambrian iron-ore basins and are their important geological constituent. These rocks are spread particularly widely in Paleoproterozoic basins, such as Hamersley in Western Australia, Transvaal in South Africa, and KMA in Russia. These vast iron–siliceous formations contain much riebeckite and crocidolite (an asbestosiform variety of riebeckite). The Brockman Formation, Hamersley basin, contains the Earth’s largest amounts of this alkali amphibole. The evaluated crocidolite reserves (exclusive of non-asbestosiform riebeckite) are close to 2.41 mln. tons (Trendall and Blockley, 1970). Vast volumes of rocks with riebeckite were also found in the Criquatown, Kuruman, and Penge formations of the Transvaal Supergroup (Miyano and Beukes, 1997).

The two currently most popular hypotheses advanced to account for the genesis of riebeckite and aegirine BIF are as follows. Some researchers (Glagolev, 1966; Trendall and Blockley, 1970) were prone to relate the origin of aegirine and riebeckite to alkaline (sodic) metasomatism, which was responsible for Na introduction into the system with fluids (the system was thereby believed to be initially poor in alkalis). No Na-rich minerals that could be precursor of riebeckite and aegirine have ever been found in low-temperature BIF. Some observations are, however, at variance with this viewpoint. Aegirine- and riebeckite-bearing BIF completely preserve their typical structures (thin banding and crenulation) but bear no metasomatic bodies of massive or impregnated structure. The riebeckite and aegirine occur in assemblages with quartz, magnetite, hematite, stilpnomelane, carbonates, tetriferrribiotite, and celadonite, i.e., there are absolutely no mono- and bimineralic assemblages. These facts give rise to certain constraints imposed onto the metasomatic model (Glagolev, 1966; Trendall and Blockley, 1970): alkaline metasomatism occurred only within zones of elevated permeability to fluids (fracturing, shattering, fault

Table 5. Composition (wt %) of aegirine-augite in BIF from the Lebedinskoe deposit (sample L-6)

Component	Fig. 7a		Fig. 7c	
	Aeg-Aug-4	Aeg-Aug-8	Aeg-Aug-28	Aeg-Aug-39
SiO ₂ , wt %	53.95	53.84	54.03	53.53
Al ₂ O ₃	–	–	–	–
FeO	24.79	27.36	23.47	23.66
MgO	4.97	3.45	5.41	5.84
CaO	8.23	6.18	9.15	7.72
Na ₂ O	8.97	10.17	8.61	8.54
Total	100.91	101.00	100.67	99.29
Si, f.u.	1.99	1.99	2.00	2.00
Al	–	–	–	–
Fe ³⁺	0.65	0.75	0.62	0.61
Fe ²⁺	0.11	0.10	0.10	0.13
Mg	0.27	0.19	0.30	0.33
Ca	0.33	0.24	0.36	0.31
Na	0.64	0.73	0.62	0.62
X _{Mg}	0.71	0.66	0.74	0.71
Aeg	64.44	73.11	61.76	61.82
Aug	35.56	26.89	38.24	38.18

zones and the like), and the intensity of this process was generally low. Because of this, Glagolev (1966) proposed to refer to the limited alkaline metasomatism of BIF as alkaline metamorphism.

The proponents of the other concept believe that riebeckite and aegirine BIF were formed by the isochemical metamorphism of a sedimentary protolith that had been produced by the sedimentation and diagenesis of aqueous Fe- and Si-rich gels, which had been enriched in Na and K (French, 1973; Klein, 1974). As this material started to crystallize during diagenesis, cation diffusion was activated, and Na and K could be incorporated into micas and riebeckite. Eugster (1969) suggested, by analogy with Pleistocene siliceous lacustrine deposits, that the siliceous deposits of BIF originally contained magadiite, a Na silicate of the composition $\text{NaSi}_7\text{O}_{13} \cdot 3\text{H}_2\text{O}$. Reactions with Fe-rich mixed-layer phyllosilicates were favorable for Na release and the formation of riebeckite (Miyano, 1982). This viewpoint finds support in riebeckite finds as an authigenic and/or very low-temperature mineral in several BIF (Lesher, 1978; Klein, 1983; Miyano and Klein, 1983). In the

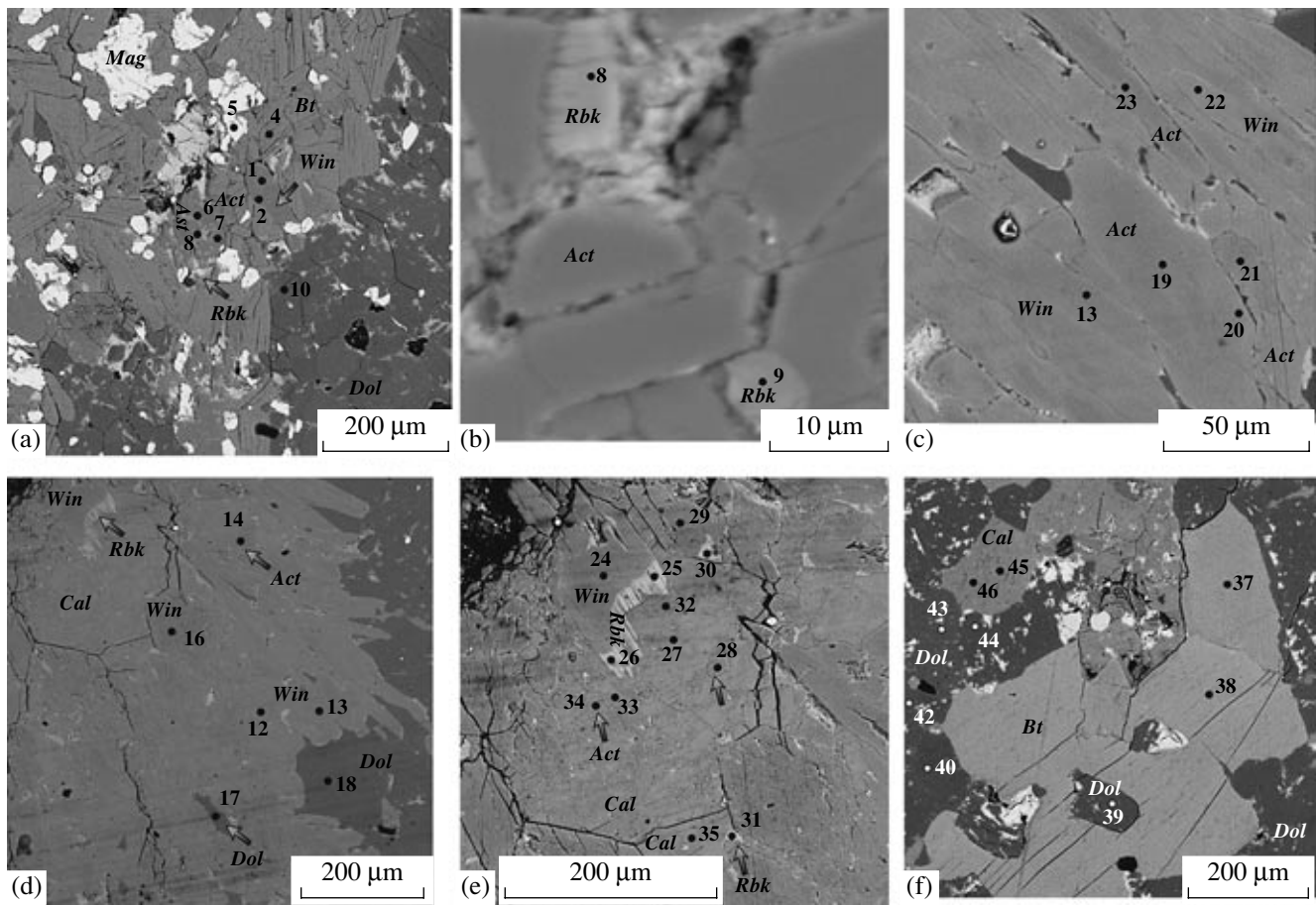


Fig. 8. Mineral assemblages and microprobe analytical spots in BIF with alkali amphiboles, sample L-2.

(a) Amphibole and dolomite layers in BIF; (b) small riebeckite crystals in an actinolite matrix; (c) absence of optical boundaries between the actinolite cores and ferriwinchite outer zones of amphibole crystals; (d) relations between riebeckite, ferriwinchite, and actinolite in an amphibole layer; (e) riebeckite rims around ferriwinchite; (f) relations between calcite and dolomite in carbonate layers.

Eocene lacustrine deposits of the Green River Formation, riebeckite, crocidolite, and aegirine are early diagenetic minerals that crystallized at a temperatures lower than 100°C, and the riebeckite overgrowths early detrital grains of brown volcanic hornblende (Eugster, 1969). Riebeckite was found, together with quartz, magnesian calcite, palygorskite, illite, and microcline, at a depth of 1.8 m in the core of a borehole drilled through the modern sediments of the deep part (668 m) of Issyk-Kyl' Lake, Kyrgyzstan (Gilart et al., 2001).

This model is, however, in conflict with the fact that BIF contain reaction textures in which riebeckite replaces grunerite (Miyano and Beukes, 1997; Savko and Kal'mutskaya, 2002), ferriwinchite, and actinolite (this publication) and is younger than the other amphiboles.

Our data indicate that riebeckite in BIF was more probably formed during the prograde metamorphic stage, with the participation of a fluid insignificantly

enriched in Na⁺ and at increasing oxygen fugacity. The formation of riebeckite with 5–6 wt % Na₂O requires relatively low Na concentrations in BIF. For example, the origin of 10 modal % riebeckite requires as little as 0.5–0.6 wt % Na₂O in the rock, although aegirine-bearing varieties need almost twice higher Na concentrations.

During early metamorphic stages, the rocks contained stable amphiboles usual in BIF: grunerite and actinolite. Because there is no complete isomorphic series between grunerite and riebeckite (Oba and Nicholls, 1986), a temperature increase results in the oxidation of grunerite and its replacement by riebeckite itself, without intermediate products (only grunerite relics in riebeckite are preserved): $2Gru + 2O_2 + 2Na^+ \rightarrow Rbk + 3Mag + 8Qtz + 2H^+$ (Miyano and Beukes, 1987). The oxidation of actinolite in the presence of Na⁺-enriched fluid produces ferriwinchite

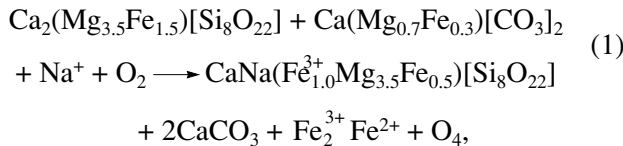
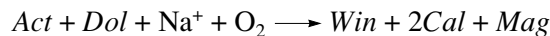
Table 6. Composition (wt %) of amphiboles from sample L-2

Component	Fig. 8a				Fig. 8b		Fig. 8d			Fig. 8c	Fig. 8c	
	Win-1	Win-2	Win-6	Win-7	Rbk-8	Rbk-9	Win-12	Win-13	Act-14	Win-16	Act-19	
SiO ₂ , wt %	56.38	56.20	56.29	56.10	54.64	54.11	57.08	57.55	57.29	56.85	57.11	
Al ₂ O ₃	—	—	0.81	—	—	—	0.62	—	—	0.70	—	
FeO	13.27	13.24	12.72	12.14	30.10	28.33	13.30	10.72	10.01	11.41	10.22	
MgO	16.22	16.13	16.35	16.73	6.03	6.79	16.09	18.13	18.43	17.32	18.43	
CaO	8.90	9.60	9.58	10.21	0.74	0.72	8.91	10.01	10.69	9.37	10.86	
Na ₂ O	2.83	2.68	2.34	1.90	6.62	7.10	2.50	2.09	1.48	2.41	1.77	
Total	97.60	97.85	98.09	97.08	98.13	97.05	98.50	98.50	97.90	98.06	98.39	
Si, f.u.	8.00	8.00	7.94	8.00	8.00	8.00	7.99	8.00	8.00	7.95	7.97	
Al ^{IV}	—	—	0.06	—	—	—	0.01	—	—	0.05	—	
Fe ³⁺	—	—	—	—	—	—	—	—	—	—	0.03	
ΣT	8.00	8.00	8.00	8.00	8.00	8.00	8.00	8.00	8.00	8.00	8.00	
Al ^{VI}	—	—	0.07	—	—	—	0.09	—	—	0.07	—	
Fe ³⁺	0.52	0.32	0.46	0.36	1.88	1.73	0.57	0.45	0.40	0.53	0.29	
Fe ²⁺	1.05	1.25	1.03	1.09	1.80	1.77	0.98	0.79	0.76	0.80	0.87	
Mg	3.43	3.42	3.43	3.55	1.32	1.50	3.35	3.75	3.83	3.61	3.83	
ΣC	5.00	4.99	4.99	5.00	5.00	5.00	4.99	4.99	4.99	5.01	4.99	
Ca	1.35	1.46	1.45	1.56	0.12	0.11	1.34	1.49	1.60	1.40	1.62	
Na	0.65	0.544	0.55	0.44	1.88	1.89	0.66	0.51	0.40	0.60	0.38	
ΣB	2.00	2.00	2.00	2.00	2.00	2.00	2.00	2.00	2.00	2.00	2.00	
Na _A	0.13	0.20	0.11	0.08	—	0.14	0.02	0.05	—	0.05	0.10	
X _{Mg}	0.765	0.732	0.767	0.765	0.422	0.458	0.773	0.826	0.833	0.819	0.815	
Component	Fig. 8c				Fig. 8e			Fig. 8e				
	Win-20	Win-21	Win-22	Act-23	Win-24	Rbk-25	Rbk-26	Win-28	Win-29	Win-34	Rbk-30	Rbk-31
SiO ₂	56.99	56.70	56.77	57.05	56.50	54.49	54.90	56.45	57.14	56.43	54.80	54.30
Al ₂ O ₃	—	—	—	—	—	—	—	—	—	0.56	—	—
FeO	12.69	11.21	13.84	9.90	11.23	32.18	29.54	10.73	11.02	13.99	29.49	28.66
MgO	16.93	17.49	16.15	18.40	17.42	4.81	6.46	17.66	18.10	16.11	6.45	6.70
CaO	9.22	10.26	8.79	11.43	9.55	0.62	0.80	10.68	9.81	8.78	0.73	0.79
Na ₂ O	2.18	1.95	2.54	1.26	2.46	6.01	6.61	2.10	2.37	2.62	6.59	6.60
Total	98.01	97.61	98.09	98.04	97.16	98.11	98.31	97.62	98.44	98.49	98.06	97.05
Si	7.98	8.00	7.99	8.00	8.00	8.00	8.00	8.00	7.96	7.91	8.00	8.00
Al ^{IV}	—	—	—	—	—	—	—	—	—	0.09	—	—
Fe ³⁺	0.02	—	0.01	—	—	—	—	—	0.04	—	—	—
ΣT	8.00	8.00	8.00	8.00	8.00	8.00	8.00	8.00	8.00	8.00	8.00	8.00
Al ^{VI}	—	—	—	—	—	—	—	—	—	—	—	—
Fe ³⁺	0.66	0.36	0.67	0.23	0.43	2.09	1.88	0.18	0.47	0.74	1.90	1.86
Fe ²⁺	0.81	0.96	0.95	0.93	0.90	1.86	1.72	1.09	0.77	0.89	1.69	1.67
Mg	3.53	3.68	3.39	3.84	3.67	1.05	1.40	3.73	3.76	3.36	1.40	1.47
ΣC	5.00	5.00	5.01	5.00	5.00	5.00	5.00	5.00	5.00	4.99	4.99	5.00
Ca	1.38	1.55	1.32	1.72	1.45	0.10	0.12	1.62	1.46	1.32	0.11	0.12
Na	0.59	0.45	0.68	0.28	0.55	1.71	1.87	0.38	0.54	0.68	1.86	1.88
ΣB	1.97	2.00	2.00	2.00	2.00	1.81	1.99	2.00	2.00	2.00	1.97	2.00
Na _A	—	0.08	0.01	0.06	0.12	—	—	0.20	0.10	0.03	—	—
X _{Mg}	0.814	0.793	0.782	0.805	0.804	0.362	0.450	0.773	0.829	0.790	0.453	0.469

Table 7. Metamorphic temperatures estimated by the calcite–dolomite thermometer for BIF in sample L-6 from the Lebedinskoe deposit

Calcite–dolo- mite pair	Temperature, °C				
	Calcite–dolomite thermometer				T_{av} , °C
	1	2	3	4	
Cal(35)–Dol(10)	403	445	442	421	428
Cal(32)–Dol(11)	422	459	454	438	443
Cal(33)–Dol(18)	403	434	428	420	421
Cal(42)–Dol(43)	367	396	366	388	379

Note: Calcite–dolomite thermometers: 1—(Puhan, 1979); 2—(Talantsev, 1981); 3—(Anovitz and Essene, 1984); 4—(Patrick and Evans, 1989).



and ferriwinchite is replaced by riebeckite

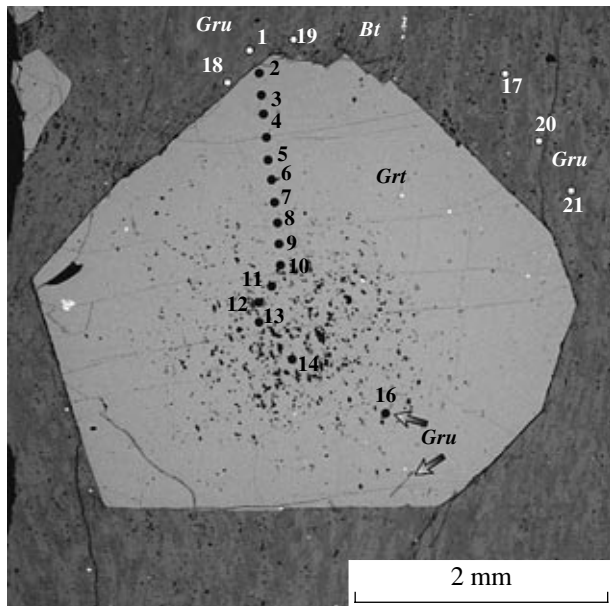
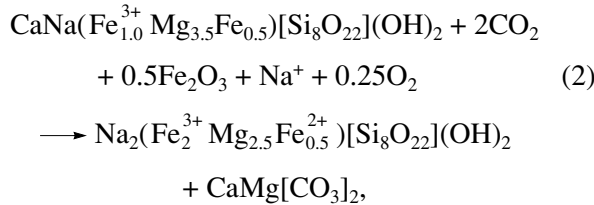
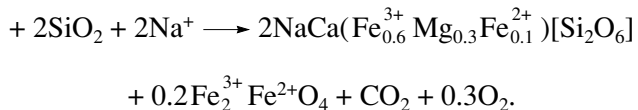
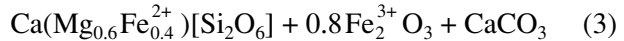
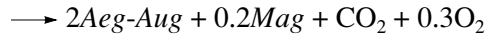
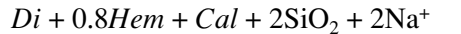


Fig. 9. Garnet porphyroblast in a fine-grained quartz–grunerite–biotite schist from the lower schist subformation (sample L-20).

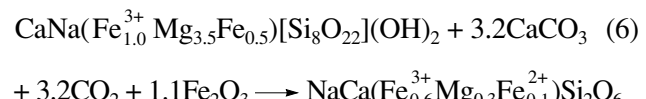
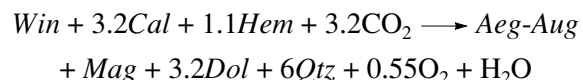
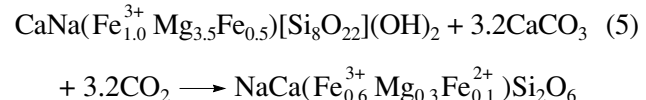
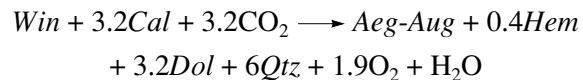
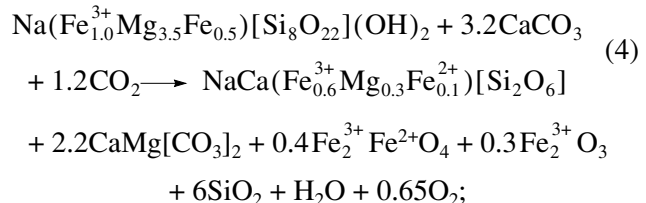
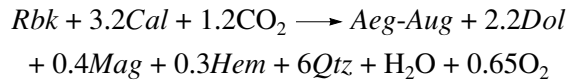
which also follows from the zoning of amphibole crystals and the broad development of carbonates (which are “byproducts” of these replacement reactions).

A further temperature increase results in the formation of aegirine-augite, a Ca–Na pyroxene, in the carbonate-bearing BIF. This mineral can be produced in two ways. First, diopside is formed in these rocks by the well known reaction $Act + Cal + Qtz \longrightarrow Di + H_2O + CO_2$ and is then replaced by aegirine-augite in the presence of Na^+ -rich fluid



There is a continuous series of solid solutions between diopside and Ca–Na pyroxene (Cameron and Papike, 1981; Morimoto, 1989).

The alternative variant is the origin of aegirine-augite by the partial decomposition of riebeckite or ferriwinchite



which is confirmed by the presence of small amounts (2–5 modal %) of hematite in the pyroxene-bearing mineral assemblages and the wide development of dolomite.

Table 8. Composition (wt %) of garnets from the lower schist subformation of the Lebedinskoe deposit (sample L-20; Fig. 9)

Component	Marginal zone			Intermediate zone without inclusions					Core with inclusions			
	Grt-2	Grt-3	Grt-4	Grt-5	Grt-6	Grt-7	Grt-8	Grt-9	Grt-10	Grt-11	Grt-12	Grt-13
SiO ₂ , wt %	36.47	36.55	36.51	36.45	36.62	36.68	36.70	36.75	36.67	36.77	36.71	36.55
Al ₂ O ₃	20.65	20.52	20.55	20.49	20.52	20.67	20.62	20.64	20.72	20.64	20.69	20.54
FeO	41.16	40.99	41.15	41.76	41.33	41.31	41.05	40.98	41.25	41.10	41.21	40.98
MnO	—	—	—	—	—	—	—	—	—	—	—	—
MgO	1.51	1.66	1.47	1.21	1.32	0.93	1.38	1.37	1.11	1.12	1.04	1.27
CaO	1.12	0.98	1.12	1.01	1.16	0.94	1.05	0.97	1.01	1.07	1.15	1.61
Total	100.91	100.70	100.80	100.92	100.95	100.53	100.80	100.71	100.76	100.70	100.80	100.95
Si, f.u.	2.971	2.980	2.977	2.977	2.983	2.998	2.988	2.993	2.989	2.997	2.992	2.978
Al	1.982	1.972	1.975	1.972	1.970	1.991	1.979	1.981	1.991	1.983	1.987	1.972
Fe	2.804	2.795	2.806	2.852	2.816	2.823	2.795	2.791	2.812	2.802	2.809	2.792
Mn	—	—	—	—	—	—	—	—	—	—	—	—
Mg	0.183	0.202	0.179	0.147	0.160	0.113	0.168	0.166	0.135	0.136	0.126	0.154
Ca	0.092	0.086	0.098	0.088	0.101	0.082	0.092	0.085	0.088	0.093	0.100	0.141
Alm	0.909	0.907	0.910	0.924	0.915	0.935	0.915	0.917	0.926	0.924	0.925	0.905
Prp	0.059	0.065	0.058	0.048	0.052	0.038	0.055	0.055	0.044	0.045	0.042	0.050
Grs	0.032	0.028	0.032	0.029	0.033	0.027	0.030	0.028	0.029	0.031	0.033	0.046
X _{Fe}	0.939	0.933	0.940	0.951	0.946	0.961	0.943	0.944	0.954	0.954	0.957	0.948

Table 9. Composition (wt %) of biotite from the lower schist subformation of the Lebedinskoe deposit (sample L-20, Fig. 9)

Component	Bt-17	Bt-18	Bt-19	Bt-20
SiO ₂ , wt %	32.55	34.40	34.73	34.36
Al ₂ O ₃	16.92	15.70	16.56	17.01
TiO ₂	1.41	1.57	1.77	1.55
FeO	31.10	28.08	26.03	26.36
MnO	—	—	—	—
MgO	7.89	7.44	7.55	7.41
CaO	—	—	0.13	—
Na ₂ O	0.08	0.08	0.28	—
K ₂ O	6.54	9.04	9.11	9.49
F	0.33	—	—	—
Cl	0.16	0.13	0.10	0.10
Total	96.98	96.44	96.26	96.28
Si, f.u.	2.573	2.716	2.716	2.695
Al ^{IV}	1.427	1.284	1.284	1.305
Al ^{VI}	0.149	0.177	0.243	0.267
Ti	0.084	0.093	0.104	0.091
Fe ²⁺	2.056	1.854	1.703	1.729
Mn	—	—	—	—
Mg	0.930	0.876	0.880	0.866
Ca	—	—	0.011	—
Na	0.012	0.012	0.042	—
K	0.660	0.910	0.909	0.949
F	0.082	—	—	—
Cl	0.021	0.017	0.013	0.13
X _{Fe}	0.689	0.679	0.659	0.666

Table 10. Metamorphic temperatures estimated by the garnet–biotite thermometer for the intramineral schists of sample L-20 from the Lebedinskoe deposit, KMA

Garnet–biotite pair (analysis numbers are the same as in Tables 8 and 9 and in Fig. 9)	<i>P</i> , kbar	Temperature, °C						<i>T</i> _{av} , °C	
		Geothermometer							
		1	2	3	4	5	6		
Grt(13)–Bt(20)	3	473	476	518	491	495	453	484	
Grt(3)–Bt(18)	3	544	539	576	548	568	534	552	
Grt(6)–Bt(17)	3	501	500	540	513	528	482	511	
Grt(2)–Bt(19)	3	502	501	520	514	520	482	507	

Note: Geothermometers: 1—(Thompson, 1976); 2—(Holdaway and Lee, 1977); 3—(Lavrent'eva and Perchuk, 1981); 4—(Perchuk, 1989); 5—(Ganguly and Saxena, 1984); 6—(Hodges and Spear, 1982).

CONCLUSIONS

Our data on the textural relations between and compositional variations of calcic, calcic–sodic, and sodic alumina-free amphiboles testify to the complete miscibility in the actinolite–ferriwinchite and ferriwinchite–riebeckite isomorphic series.

All reaction textures examined in the rocks were formed during the prograde metamorphic stage, at peak metamorphic temperatures of about 550°C, and were a succession of mineral replacements, such as *Gru* → *Rbk*, *Act* → *Win* → *Rbk*. Aegirine-augite was formed at temperatures close to the metamorphic peak by the partial decomposition of riebeckite and ferriwinchite.

The critical factors that controlled the development of alkaline amphiboles in the carbonate-bearing BIF were oxygen fugacity and the presence of even insignificant concentrations of Na ions in the fluid. These minerals contain Fe³⁺, and all reactions producing them are oxidation reactions. The crystallization of riebeckite late in the mineral-forming process was caused by the heterovalent substitution Ca²⁺Mg²⁺ → Na⁺Fe³⁺ in calcic and calcic–sodic amphiboles and by the oxidation of grunerite in the presence of a fluid enriched in Na ions. Na is characterized by chemical affinity to Fe³⁺, which explains why natural rocks often contain riebeckite and aegirine but never bear alumina-free potassio amphiboles or pyroxenes. In oxidizing environments, Na⁺ is readily accommodated in Al-free amphiboles and pyroxene in place of Fe³⁺.

ACKNOWLEDGMENTS

The author thanks D.I. Kosarev, Deputy Chief Geologist of the Lebedinskii Mining and Processing Plant for help with fieldwork. This study was financially supported by the Russian Foundation for Basic Research, project no. 06-05-64088.

REFERENCES

- L. M. Anovitz and E. J. Essene, “Phase Equilibria in the System CaCO₃–MgCO₃–FeCO₃,” *J. Petrol.* **28** Pt. 2, 389–414 (1987).
- G. V. Artemenko, Doctoral Dissertation in Geology and Mineralogy (Kiev, 1998) [in Russian].
- M. Cameron and J. J. Papike, “Structural and Chemical Variations in Pyroxenes,” *Am. Mineral.* **66** (1/2), 1–50 (1981).
- H. P. Eugster, “Inorganic Bedded Cherts from the Magadi Area, Kenya,” *Contrib. Mineral. Petrol.* **22**, 1–31 (1969).
- V. I. Fonarev, A. A. Graphchikov, and A. N. Konilov, “A Consistent System of Geothermometers for Metamorphic Complexes,” *Int. Geol. Rev.* **33** (8), 743–783 (1991).
- B. M. French, “Mineral Assemblages in Diagenetic and Low-Grade Metamorphic Iron Formations,” *Econ. Geol.* **68**, 1063–1074 (1973).
- J. Ganguly and S. K. Saxena, “Mixing Properties of Aluminosilicate Garnets: Constraints from Natural and Experimental Data, and Applications to Geothermobarometry,” *Am. Mineral.* **69** (1/2), 88–97 (1984).
- S. Ghose, W. C. Forbes, and P. P. Phakey, “Unmixing of an Alkali Amphibole (Tirodite) Into Magnesio-Richerite and Magnesio-Riebeckite,” *Indian J. Earth Sci.*, No. 1, 37–42 (1974).
- S. Giralt, S. Riera, J. Klerkx, et al., “Lake Issyk-Kul: An Example of Recent Evolution in a Continental Environment,” in *Proceedings of 3rd Workshop Southern European Working Group of the European Lake Drilling, Girona, Spain, 2001*, Terra Nostra, No. 1/2, 30–36 (2001).
- A. A. Glagolev, *Metamorphism of the Precambrian Rocks of KMA* (Nauka, Moscow, 1966) [in Russian].
- M. J. Gole and C. Klein, “Banded Iron Formation through Much of Precambrian Time,” *J. Geol.* **89**, 169–183 (1981).
- K. V. Hodges and F. S. Spear, “Geothermometry, Geobarometry and the Al₂SiO₅ Triple Point at Mt. Moosilauke, New Hampshire,” *Am. Mineral.* **67** (11/12), 1118–1134 (1982).
- M. J. Holdaway and S. M. Lee, “Fe–Mg Cordierite Stability in High Grade Pelitic Rocks, Based on Experiments,” *Am. Mineral.* **73** (11/12), 1118–1134 (1988).

- tal, Theoretical and Natural Observations," Contrib. Mineral. Petrol. **63** (2), 175–198 (1977).
14. *Iron Ores of KMA*, Ed. by V. P. Orlov et al. (Geoinform-mark, Moscow, 2001) [in Russian].
 15. H. L. James, "Sedimentary Facies of Iron Formation," Econ. Geol. **49**, 235–285 (1954).
 16. C. Klein, "Greenalite, Minnesotaite, Crocidolite and Carbonates in a Very Low-Grade Metamorphic Precambrian Iron Formation," Can. Mineral. **12**, 475–498 (1974).
 17. C. Klein, "Two-Amphibole Assemblages in the System Actinolite–Hornblende–Glauophane," Am. Mineral. **54**, 212–237 (1969).
 18. C. Klein, "Diagenesis and Metamorphism of Precambrian Iron Formations," in *Iron Formations: Facts and Problems*, Ed. by A. F. Trendall and R. C. Morris (Elsevier, Amsterdam, 1983), pp. 417–469.
 19. I. V. Lavrent'eva and L. L. Perchuk, "Phase Relations in the Biotite–Garnet System. Experimental Data," Dokl. Akad. Nauk SSSR **260** (3), 731–734 (1981).
 20. B. E. Leake and A. R. Woolley, and 20 Members of the Subcommittee on Amphiboles, "Nomenclature of Amphiboles. Report of the Subcommittee on Amphiboles of the International Mineralogical Association Commission on New Minerals and Mineral Names," Eur. J. Mineral **9**, 623–651 (1997).
 21. C. M. Lesher, "Mineralogy and Petrology of the Sokoman Iron Formation Near Ardua Lake, Quebec," Can. J. Earth Sci. **15**, 480–500 (1978).
 22. T. Miyano and C. Klein, "Conditions of Riebeckite Formation in the Iron-Formation of the Dales Gorge Member, Hamersley Group, Western Australia," Am. Mineral. **68**, 517–529 (1983).
 23. T. Miyano and N. J. Beukes, "Mineralogy and Petrology of the Contact Metamorphosed Amphibole Asbestos-Bearing Penge Iron Formation, Eastern Transvaal, South Africa," J. Petrol. **38** (5), 651–676 (1997).
 24. T. Miyano, "Stilpnomelane, Fe-Rich Mica, K-Feldspar and Hornblende in Banded Iron Formation Assemblages of the Dales Gorge Member, Hamersley Group, Western Australia," Can. Mineral. **20**, 189–202 (1982).
 25. N. Morimoto, "Nomenclature of Pyroxenes. Report of the Subcommittee on Pyroxenes of the International Mineralogical Associations on New Minerals and Mineral Names," Can. Mineral. **27**, 143–156 (1989).
 26. T. Oba and I. A. Nicholls, "Experimental Study of Cummingtonite and Ca–Na Amphibole Relations in the System *Gru–Act–Pl–Qtz–H₂O*," Am. Mineral. **71**, 1354–1365 (1986).
 27. B. E. Patric and B. W. Evans, "Metamorphic Evolution of the Seward Peninsula Blueschist Terrane," J. Petrol. **30** (3), 531–555 (1989).
 28. L. L. Perchuk, "Consistency between Some Fe–Mg Geothermometer based on the Nernst Law: Revision," Geokhimiya, No. 5, 611–622 (1989).
 29. N. A. Plaksenko, *Principal Relations and Tendencies of Iron Sedimentation in the Precambrian* (Voronezhsk. Univ., Voronezh, 1966) [in Russian].
 30. D. Puhan, *Petrographie und Geothermometrische Untersuchungen an Silicat Führenden Dolomit–Calcit–Marmoren zur Ermittlung der Metamorphose Bedingungen im Zentral-Damara-Orogen (SW-Africa)* (Univ. Gottingen, Habil., 1979).
 31. B. Reynard and M. Ballevre, "Coexisting Amphiboles in an Eclogite from the Western Alps: New Constraints on the Miscibility Gap Between Sodic and Calcic Amphiboles," J. Metamorph. Geol. **6**, 333–350 (1988).
 32. P. Robinson, F. S. Spear, J. C. Schumacher, et al., "Phase Relations of Metamorphic Amphiboles: Natural Occurrence and Theory," Rev. Mineral. **9B**, 1–201 (1982).
 33. K. A. Savko and M. V. Poskryakova, "Mineralogy, Phase Equilibria, and Metamorphism of the Rocks of the Novoyaltinskoe Iron Deposit of KMA," Vestn. Voronezhsk. Univ., Ser. Geol., No. 2, 113–130 (2003a).
 34. K. A. Savko and M. V. Poskryakova, "Mineralogy, Phase Equilibria, and Metamorphism of the Shemraevskoe Iron Deposit of the Kursk Magnetic Anomaly," Vestn. Voronezhsk. Univ., Ser. Geol., No. 1, 68–84 (2004).
 35. K. A. Savko and M. V. Poskryakova, "Riebeckite–Aegirine–Celadonite BIF at the Mikhailovskoe Iron Deposit of the Kursk Magnetic Anomaly: Phase Equilibria and Metamorphic Conditions," Petrologiya **11**, 471–490 (2003b) [Petrology **11**, 426–443 (2003)].
 36. K. A. Savko and N. Yu. Kal'mutskaya, "Physicochemical Conditions of Metamorphism of the Magnetite–Grunerite–Riebeckite Rocks of the Priorskolskoe Iron Deposit of the Kursk Magnetic Anomaly," Vestn. Voronezhsk. Univ., Ser. Geol., No. 1, 95–103 (2002).
 37. I. N. Shchegolev, *Precambrian Ore Deposits and Methods of their Study* (Nedra, Moscow, 1985) [in Russian].
 38. N. P. Shcherbak, G. V. Artemenko, E. N. Bartnitskii, et al., "Age of Silicic Metavolcanic Rocks of the Aleksandrovskii and Korobkovskii Areas of KMA," Dokl. Akad. Nauk Ukr. SSR: Ser. B, No. 6, 120–123 (1992).
 39. C. K. Shearer, J. C. Schumacher, and P. Robinson, "Zoned Hastingsite–Ferri-Katophorite–Taramite Phenocrysts, an Amphibole + Orthoclase = Aegirine–Augite + Biotite Reaction, and a New Sodic Amphibole in Nepheline–Sodalite Syenite, Red Hill, New Hampshire," Geol. Soc. Amer. Abstr. **13**, 552 (1981).
 40. E. A. Smelik and D. R. Veblen, "Exsolution of Ca-Amphibole from Glauophane and the Miscibility Gap Between Sodic and Calcic Amphiboles," Contrib. Mineral. Petrol. **112**, 178–195 (1992).
 41. A. S. Talantsev, *Geothermobarometry on Dolomite–Calcite Assemblages* (Nauka, Moscow, 1981) [in Russian].
 42. A. B. Thompson, "Mineral Reactions in Pelitic Rocks: 1. Prediction of *P–T–X* (Fe–Mg) Relations," Am. J. Sci. **276** (4), 401–424 (1976).
 43. A. F. Trendall and J. G. Blockley, "The Iron Formation of the Precambrian Hamersley Group, Western Australia with Special Reference to the Associated Crocidolite," Geol. Surv. W. Aust. Bull. (1970).